Chloroplasts lacking class I glutaredoxins are functional but show a delayed recovery of protein cysteinyl redox state after oxidative challenge

Finja Bohle[1,2], Jacopo Rossi[3], Sadia S. Tamanna[1], Hannah Jansohn[1], Marlene Schlosser[1], Frank Reinhardt[4], Alexa Brox[5], Stephanie Bethmann[6], Stanislav Kopriva[7], Oliver Trentmann[1], Peter Jahns[6], Marcel Deponte[8], Markus Schwarzländer[9], Paolo Trost[3], Mirko Zaffagnini[3], Andreas J. Meyer[2], Stefanie J. Müller-Schüssele[1*]

[1] Molecular Botany, Department of Biology, RPTU Kaiserslautern-Landau, D-67633 Kaiserslautern, Germany

[2] Chemical Signalling, Institute of Crop Science and Resource Conservation (INRES), University of Bonn, D-53113 Bonn, Germany

[3] Department of Pharmacy and Biotechnology, University of Bologna, I-40126 Bologna, Italy

[4] Plant Physiology, Department of Biology, RPTU Kaiserslautern-Landau, D-67633 Kaiserslautern, Germany

[5] Crop Functional Genomics, Institute of Crop Science and Resource Conservation (INRES), University of Bonn, D-53113 Bonn, Germany

[6] Plant Biochemistry, Heinrich-Heine-University Düsseldorf, D-40225 Düsseldorf, Germany

[7] Institute for Plant Sciences, Cluster of Excellence on Plant Sciences (CEPLAS), University of Cologne, Cologne 50674, Germany

[8] Biochemistry, Department of Chemistry, RPTU Kaiserslautern-Landau, D-67633 Kaiserslautern, Germany

[9] Institute of Plant Biology and Biotechnology, University of Münster, D-48143 Münster, Germany

Short title: Chloroplasts lacking class I GRX

***Correspondence**:
Stefanie Müller-Schüssele
Rheinland-Pfälzische Technische Universität Kaiserslautern Landau (RPTU)
Erwin-Schrödinger-Str. 70
67663 Kaiserslautern
mueschue@rptu.de
Tel.: +49 (0)631-205-4391
Fax: +49 (0)631-205-2998

ORCIDs: FB: 0000-0001-8343-1399; SST: 0000-0001-7444-6222; FR: 0000-0001-6725-1793; SK: 0000-0002-7416-6551; PJ: 0000-0002-5340-1153; MS: 0000-0003-0796-8308; PT: 0000-0002-6347-8701; MZ: 0000-0001-5115-0859; AJM: 0000-0001-8144-4364; SJM-S: 0000-0003-4061-1175

Keywords: glutaredoxin, GRXC5, *S*-glutathionylation, redox-sensitive GFP, E_{GSH}, genetically encoded biosensor, photosynthesis, plastid, glutathione

One sentence summary: Removal of class I GRX activity in the chloroplast stroma of *P. patens* kinetically uncouples GRX-dependent cysteine redox changes from the local glutathione redox potential, without an effect on NPQ or photosynthetic carbon reactions.

Abstract

Redox status of protein cysteinyl residues is mediated via glutathione (GSH)/glutaredoxin (GRX) and thioredoxin (TRX)-dependent redox cascades. An oxidative challenge can induce post-translational protein modifications on thiols, such as protein *S*-glutathionylation. Class I GRX are small thiol-disulfide oxidoreductases that reversibly catalyse *S*-glutathionylation and protein disulfide formation. TRX and GSH/GRX redox systems can provide partial backup for each other in several subcellular compartments, but not in the plastid stroma where TRX/light-dependent redox regulation of primary metabolism takes place. While the stromal TRX system has been studied at detail, the role of class I GRX on plastid redox processes *in vivo* is still unknown. We generate knockout lines of *GRXC5* as the only chloroplast class I GRX of the moss *Physcomitrium patens*.

While we find that class I PpGRXC5 has high activities in glutathione-dependent oxidoreductase assays using hydroxyethyl disulfide or redox-sensitive GFP2 (roGFP2) as substrates *in vitro*, Δ*grxc5* plants show no detectable growth defect or stress sensitivity, in contrast to mutants with a less negative stromal E_{GSH} (Δ*gr1*). Using stroma-targeted roGFP2, we show increased protein Cys oxidation and decreased reduction rates after oxidative challenge in Δ*grxc5* plants *in vivo*, indicating kinetic uncoupling of the protein Cys redox state from glutathione redox potential. Protein Cys disulfide and *S*-glutathionylation formation rates after H_2O_2 treatment remained unchanged. Lack of class I GRX function in the stroma did not result in impaired carbon fixation.

Our observations suggest specific roles for class I GRX in the efficient redox equilibration between E_{GSH} and protein Cys in the plastid stroma as well as negligible cross-talk with metabolic regulation via the TRX system. We propose a model for stromal class I GRX function as efficient kinetic couplers of protein Cys redox state to the dynamic stromal E_{GSH} and highlight the importance of identifying *in vivo* target proteins of GRXC5.

Introduction

Oxygenic photosynthesis has shaped our planet by increasing oxygen levels in the atmosphere, and by enabling solar-driven carbon fixation. In phototrophic eukaryotic life forms, former free-living cyanobacteria now serve as chloroplasts in light-harvesting and production of reducing equivalents to power reductive processes in cell metabolism (Schreiber et al., 2022). Land plant chloroplasts face multiple oxidative challenges as environmental conditions such as light intensity, water availability and temperature can rapidly fluctuate and cause imbalances between light reactions and carbon fixation. Plants have adapted to a frequently changing environment by evolving mechanisms to regulate photochemistry and carbon fixation in a matter of minutes, as well as mechanisms to acclimate to a changed steady state in a matter of hours or days (Roach and Krieger-Liszkay, 2014; Schöttler and Toth, 2014; Alboresi et al., 2019; Morales and Kaiser, 2020). Regulation of the enzymatic reactions of the Calvin-Benson-Bassham cycle (CBB cycle) to match the activity of the light reactions guarantees efficient re-oxidation of the electron acceptor of light reactions, $NADP^+$, and avoids futile cycling under dark conditions when the oxidative pentose phosphate pathway is active (Buchanan et al., 2012). Thus, many stromal enzymes evolved Cys-based redox-regulation (Buchanan and Balmer, 2005; Balsera et al., 2014). This regulation of protein activity or oligomerization (Marri et al., 2014) can be mediated by post-translational changes in cysteinyl thiol redox states, including the formation/reduction of regulatory disulfide bonds on target proteins (Michelet et al., 2013; Gütle et al., 2016; Gurrieri et al., 2023). The thioredoxin (TRX) system derives electrons from the photosynthetic electron transport (PET) or NADPH for the reduction of specific regulatory disulfides on metabolic enzymes (Geigenberger et al., 2017). The redox state of these thiol-switches depends on the redox state of TRXs, which in turn depend on PET/NADPH-dependent reduction rates (Zimmer et al., 2021; Teh et al., 2023) and oxidation rates (Yoshida et al., 2019). TRX oxidation rates can be linked via 2 Cys-peroxiredoxins (PRX) to the detoxification of hydrogen peroxide (H_2O_2) (Pérez-Ruiz et al., 2017; Ojeda et al., 2018; Vaseghi et al., 2018) which functions as terminal electron acceptor.

When the stromal NADP pool becomes increasingly reduced, generation of reactive oxygen species (ROS) increases (photoinhibitory conditions) as photosystem I (PSI) becomes acceptor-limited (Roach and Krieger-Liszkay, 2014). Via superoxide dismutases, superoxide is rapidly (without input of additional electrons) converted to H_2O_2 that can react with cysteine residues causing thiol oxidation, either directly (highly reactive Cys only) or via the Cys-redox relays (Deponte, 2017; Alvarez and Salinas, 2022). To balance ROS formation and repair ROS-induced oxidative damage, chloroplasts have evolved multiple detoxification and repair systems that either draw electrons from the TRX system or the glutathione system.

Glutathione (GSH) is a cysteine-containing tri-peptide present at millimolar concentrations in the cytosol and chloroplast stroma serving multiple roles in cellular metabolism and defense

(Bangash et al., 2019; Cassier-Chauvat et al., 2023). First, glutathione is an important electron donor for H_2O_2 detoxification or repair of ROS-induced damages (reviewed in Noctor et al., 2012 and Müller-Schüssele et al. (2021a)). Second, it can form mixed disulfides with cysteinyl residues in proteins (protein *S*-glutathionylation), either as a consequence of cysteine oxidation by H_2O_2 (*S*-sulfenylation), or enzymatically catalysed by class I glutaredoxins (GRXs) (**Fig. 1**) (Deponte, 2017). Class I GRXs are small oxidoreductases belonging to the TRX superfamily, that can form or release protein *S*-glutathionylation and disulfides (Fernandes and Holmgren, 2004; Lillig et al., 2008; Couturier et al., 2013; Trnka et al., 2020). *S*-glutathionylation can affect protein activity and/or oligomerization as well as act as a protection against protein Cys over-oxidation, depending on the modified protein and site (Michelet et al., 2005; Zaffagnini et al., 2007; Bedhomme et al., 2009; Zaffagnini et al., 2013). GRXs and TRXs can at least partially functionally complement each other, lack of both activities in the cytosol leads to lethality in *S. cerevisiae* (Draculic et al., 2000). Thus, the redox state of individual cysteine residues depends on an intricate network of redox reactions with partially overlapping but also specific roles for TRX, NTRC- and GSH/GRX-dependent reactions.

In the plastid stroma, the presence of a glutathione reductase (GR) leads to a highly reducing steady-state glutathione redox potential (E_{GSH}) with only nanomolar amounts of oxidized glutathione, glutathione disulfide (GSSG) (**Fig. 1**) (Yu et al., 2013; Schwarzländer et al., 2016; Marty et al., 2019; Müller-Schüssele et al., 2020). Stromal steady-state E_{GSH} monitored by the genetically encoded biosensor Grx1-roGFP2 (Meyer et al., 2007; Gutscher et al., 2008; Schwarzländer et al., 2008) revealed light-dependent redox dynamics (Müller-Schüssele et al., 2020; Haber et al., 2021).

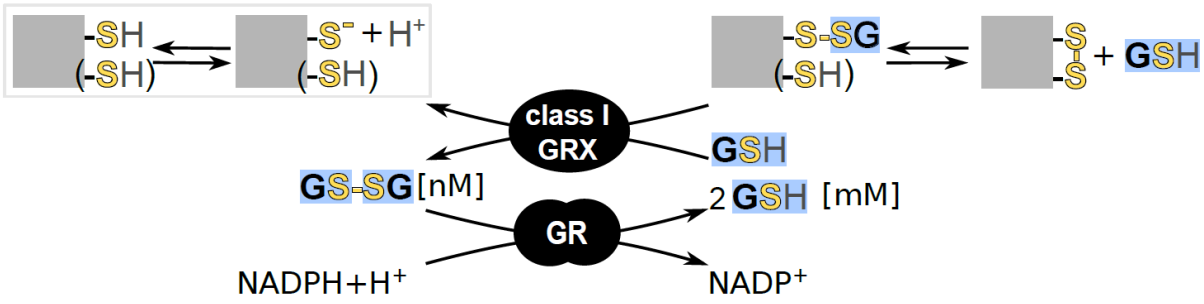

Figure 1: Scheme of class I GRX and glutathione reductase function

Class I glutaredoxins (GRX) can reversibly modify cysteinyl residues (thiol group SH, thiolate S^-) in proteins by forming a mixed disulfide with the tripeptide glutathione (GSH). If a second cysteine is present in a suitable distance, this *S*-glutathionylation can be released by intramolecular disulfide formation, as observed for the genetically encoded redox sensor roGFP2. Glutathione reductase (GR) regenerates glutathione disulfide (GSSG) to 2 glutathione (GSH) at the expense of NADPH, keeping the glutathione redox potential E_{GSH} reducing for most cysteines. Grey squares represent GRX substrate proteins, black rounded shapes enzymes.

In contrast to mitochondria and cytosol, the plastid TRX system does not constitute an effective functional backup system for the stromal GSH/GRX system, as a lack in stromal GR causes

embryo-lethality in *A. thaliana* (Marty et al., 2009; Marty et al., 2019). In the model moss *Physcomitrium patens*, plants lacking mitochondria/plastid-targeted glutathione reductase (PpGR1) had a shifted (less negative) stromal E_{GSH} and were viable, albeit dwarfed and light-sensitive (Müller-Schüssele et al., 2020). Plant class I GRX clades that contain isoforms targeted to different subcellular compartments are evolutionary conserved from bryophytes to flowering plants (Müller-Schüssele et al., 2021a). In the model flowering plant *A. thaliana*, two plastid-targeted class I GRXs exist that differ by the number of cysteines in the active site. While AtGRXS12 contains a single cysteine (WCSYS active site), AtGRXC5 contains two cysteines (YCPYC active site) (Couturier et al., 2011; Müller-Schüssele et al., 2021a). According to previous phylogenetic analysis, GRXC5 represents the ancestral type of plastid-targeted class I GRX with a single isoform of GRXC5 in the model moss *P. patens* (Müller-Schüssele et al., 2021a).

The chloroplast stroma has been described as a 'redox battle ground' (Meyer et al., 2021) of which we are still lacking a functional map. In particular, the roles of glutathione, class I GRX and protein *S*-glutathionylation are largely uncharted. It is an open question how class I GRX function and *S*-glutathionylation dynamically interact with the known thiol-switching cascades in the crucial light/dark regulation of chloroplast metabolism.

Here, we set out to understand the role of class I GRX in the stromal redox network of plants. To this end we generated plant lines lacking class I GRX activity in the stroma, by exploiting the fact that only a single plastid-targeted class I GRX present in *Physcomitrium patens.* We combine biochemical characterization of PpGRXC5 *in vitro* with *in vivo* biosensing using stroma-targeted roGFP2 to dynamically monitor protein Cys redox changes after oxidative challenge.

Material and Methods

In vitro analyses of PpGRXC5

For recombinant protein expression of PpGRXC5, *P. patens* cDNA was used to amplify *GRXC5* without targeting peptide (starting at the Ala 120 codon) using the primer combination PpGRXC5_A120_F GGGGACAAGTTTGTACAAAAAAGCAGGCTTAGCAGCAGGTT CGGGG and PpGrxC5_cds_R GGGGACCACTTTGTACAAGAAAGCTGGGTG TCAACTCCTGTTTGCACCAG, adding *attB1* and *attB2* sites. The PCR-product was cloned via Gateway™ into pDONR207, verified by sequencing, and subsequently inserted into the pETG-10A vector. Recombinant proteins (roGFP2 (Meyer et al., 2007), PpGRXC5, AtGRXC1 (AT5G63030, (Rouhier et al., 2007)) were purified from transformed *E. coli* strain *Rosetta2* as described in Trnka et al., (2020) and Ugalde et al. (2021).

Hydroxyethyl disulfide (HED) assay. Deglutathionylation activity of PpGRXC5 was tested according to Zaffagnini et al. (2008). Prior to the assay, the concentration of GRXC5 was determined via Bradford assay (Bradford, 1976). All chemicals were dissolved in 100 mM Tris-HCl pH 7.9. A 20 mM NADPH stock was prepared, and concentration was verified via absorption measurements using the NADPH extinction coefficient of 6.23 mM^{-1} cm^{-1}. To test for the GRX concentration in which the GRX shows a linear activity, HED assays were performed in 100 mM Tris-HCl, 1 mM EDTA pH 7.9 using 1 mM GSH and 0.7 mM HED, varying the concentration of the GRX from 10-50 nM. The HED assay, with GSH as variable substrate, was performed by preparing a 1 ml cuvette containing 0.5-4 mM GSH and 0.7 mM bis(2-hydroxyethyl)disulfide (HED). With HED as variable substrate, GSH concentration was kept constant at 1 mM, while HED concentrations varied from 0.3 mM to 1.5 mM. To the HED and GSH mixture 200 µM NADPH and 100 mM Tris-HCl 1 mM EDTA pH 7.9 were added. After exactly 3 min of incubation, GR (final concentration of 6 µg ml^{-1}, *Saccharomyces cerevisiae*, Sigma-Aldrich CAS 9001-48-3, 100-300 units/mg protein) and GRXC5 (final concentration 30 nM) were added to the cuvette adding up to a final volume of 1 ml. For each concentration of varying GSH or HED, a background activity was determined by replacing GRX with buffer (Tris-HCl, pH 7.9). The absorbance decrease at 340 nm was followed for 1 min using a NanoDrop™ 2000c spectrophotometer (Thermo Fisher Scientific).

roGFP2-based *in vitro* assays. Oxidation and reduction assays using roGFP2 (Meyer et al., 2007; Gutscher et al., 2008; Bohle et al., 2023) were performed in a 96-well plate in a fluorescence plate reader (CLARIOstar® Plus, BMG Labtech). For oxidized and reduced roGFP2 controls, roGFP2 was treated for 30 min with 10 mM DTT or 10 mM H_2O_2 before the assay start. To assess the reduction capacities of PpGRXC5, 1 µM of untreated (oxidized) roGFP2 was pipetted into a well containing 1 µM GRX (PpGRXC5, AtGRXC1), 100 µM NADPH and 1 unit *S. saccharomyces* GR in 100 µl of 100 mM potassium phosphate buffer pH 7.4. After measuring for 10 cycles, a final concentration of 2 mM GSH was added automatically by the injection needles of the plate reader into the respective wells. Fluorescence was followed until roGFP2 ratio stabilized. For assessing oxidation capacities of PpGRXC5, 10 µM roGFP2 was pre-reduced with 10 mM DTT for 30 min and subsequently desalted via Zeba™Spin Desalting Columns (ThermoFisher) following the manufacturer's instructions. 1 µM of pre-reduced roGFP2 was mixed with 1 µM of PpGRXC5 or AtGRXC1 in potassium phosphate buffer pH 7.4. 2 mM GSSG was added via the injection needles of the plate reader after 5 min of initial measurements and the measurement continued until roGFP2 ratio stabilized. Fluorescence intensities were collected by excitation at 390-10 nm or 480-10 nm and emission at 530-10 nm.

Plant materials and growth conditions

Physcomitrium patens (Hedw.) Bruch & Schimp ecotype 'Gransden 2004' (International Moss Stock Centre (IMSC, http://www.moss-stock-center.org), accession number 40001) was grown axenically and regularly sub-cultured in agitated liquid medium (KNOP medium: 250 mg l^{-1} KH_2PO_4, 250 mg l^{-1} KCl, 250 mg l^{-1} $MgSO_4 \times 7H_2O$,1 g l^{-1} $Ca(NO_3)_2 \times 4H_2O$ and 12.5 mg l^{-1} $FeSO_4 \times 7H_2O$, pH 5.8) (Reski and Abel, 1985) supplemented with micro-elements (ME), (H_3BO_3, $MnSO_4$, $ZnSO_4$, KI, $Na_2MoO_4 \times 2H_2O$, $CuSO_4$, $Co(NO_3)_2$). For phenotypic analyses, *P. patens* gametophores were grown on KNOP ME agar plates (12 g l^{-1} purified agar; Oxoid, Thermo Scientific, Waltham, MA, USA). Light intensity in growth cabinets was set to 70-100 µmol photons m^{-2} s^{-1} and 16:8 h light/dark cycle at 22 °C, if not indicated otherwise.

Generation of transgenic lines

Δ***grxc5***. The complete *GRXC5* (Pp3c3_7440V3.3 (V1.6 Pp1s321_10V6.1)) coding sequence (cds) was exchanged via homologous recombination with a *nptII* resistance cassette under the control of the *NOS* promoter and terminator. The knock-out construct was assembled by triple-template PCR (Tian et al., 2004), using the following primer combinations: upstream (5') homologous region (HR) PpGRXC5ko_5PHR_P1 ATCACAGGAAGCTATGGAAGGCA and PpGRXC5ko_5PHR_P2 TTGACAGGATCCGATAATCCCCACTTAGCACCAGG, resistance cassette GRXC5ko_npt_F: TGCTAAGTGGGGATTATCGGATCCTGTCAAACACTG and GRXC5ko_npt_R: CGTATGTGATGGCATGACAGGAGGCCCGATCTAGTA, downstream (3') HR PpGrxC5ko_3PHR_P3 ATCGGGCCTCCTGTCATGCCATCACATACGGAACT and PpGrxC5ko_3PHR_P4 ATCTTCAGCTCCTCAGTTCCTCG (**Table S1**). *Eco*RV restriction sites were introduced by ligating the triple-template PCR product into the pJET1.2 (Thermo Scientific, Waltham, MA, USA) vector. The resulting vector was amplified in and purified from *E. coli DH5alpha* strain, digested with *Eco*RV and used for polyethylene glycol-mediated protoplast transformation as previously described (Hohe et al., 2004). Regenerating plants surviving geneticin G418 (12.5 mg l^{-1}) selection for four weeks were further screened via PCR for homologous 5' and 3' integration of the knock-out construct at the target locus using the primer combinations GrxC5_5P_F AAGTAGGGAAAAGAGAGCACG and H3b_R CCAAACGTAAAACGGCTTGT as well as NOST_F GCGCGGTGTCATCTATGTTA and GrxC5_3P_R TGTCGTGTGTTCGGACTTCT (**Table S1**). Absence of transcript on cDNA-level was confirmed using the primer combination PpGrxC5_RT_F TTAATCGGCAGGTGTGTGGA and PpGrxC5_RT_R AAAAGCTTCTTCACGCGCAT (**Fig. S1**). Δ*grxc5* lines are available from the IMSC under the accession numbers: Δ*grxc5* #54 IMSC-Nr. 40954, Δ*grxc5* #249 IMSC-Nr. 40955). Δ*gr1* lines in Δ*grxc5* #54 genetic background were generated and identified as described in Müller-Schüssele et al. (2020), see also (**Fig. S1, Table S1**).

Plastid-targeted roGFP2. The construct of plastid-targeted roGFP2 was generated by overlap PCR. Two DNA templates were generated in separate PCR reactions adding *attB1* and *attB2*

sites to the 5' and 3' ends, respectively: the plastid transketolase targeting peptide (TKTP) sequence of *N. tabacum* (Schwarzländer et al., 2008; Speiser et al., 2018) was amplified using TKTP_F (GGGGACAAGTTTGTACAAAAAAGCAGGCTATGGCGTCTTCTTCTTCTCT) and TKTP_roGFP2_R (CCTCGCCCTTGCTCACCAGCGCAGTCTCAGTT), creating an overlap to the *roGFP2* coding sequence. Similarly, *roGFP2* was amplified with TKTP-roGFP2_F (ACTGAGACTGCGCTGGTGAGCAAGGGCGAGGAG) and roGFP2-attB2_R (GGGGACCACTTTGTACAAGAAAGCTGGGTCTTACTTGTACAGCTCGTCCATG), creating an overlap with the *TKTP* sequence (**Table S1**). The overlap PCR product was cloned by Gateway BP reaction in the pDONR207 entry vector. A clone with correct sequence was recombined via LR reaction into an expression vector (*PTA2_Act5_GW*) containing a Gateway *attR1/attR2* cassette between the *PpActin5* promoter and nopaline synthase (*NOS*) terminator, as well as homologous regions for integration at the *P. patens PTA2* locus (Kubo et al., 2013; Mueller and Reski, 2015). For protoplast transformation, the expression vector was digested with *BspQ1*, cutting at the ends of *PTA2* homologous regions, and co-transformed with a second uncut plasmid containing the *hpt* resistance cassette (pJET1.2 hpt; cds of hygromycin phosphotransferase under the control of *NOS* promoter and terminator). After four weeks of selection on hygromycin (12.5 µg ml^{-1}) (Mueller et al., 2014), two transgenic lines expressing plastid-targeted roGFP2 in Δ*grxc5#54* background (lines #17 (IMSC-Nr. 40957) and #21 (IMSC-Nr. 40958)) and one transgenic line in WT background (#20, IMSC-Nr. 40959) were used for further analyses and are available from the IMSC.

Confocal laser scanning microscopy

Microscopy was carried out as described in Müller-Schüssele et al. (2020) using a LSM780 (attached to an Axio Observer.Z1) (Carl Zeiss, Oberkochen, Germany) with 25x (Plan-Apochromat 25×/0.8 Imm Korr NA0.8) or 40x (C-Apochromat 40×/1.2W Korr NA1.2) objective. roGFP2 redox state was monitored by sequential excitation at 405 nm and 488 nm, detecting emission from 508 to 535 nm. Autofluorescence was recorded using excitation at 405 nm and emission detected from 430 to 470 nm. Chlorophyll autofluorescence was monitored after 488 nm excitation at an emission of 680 to 735 nm. Image intensities and 405/488 nm ratios were calculated per pixel using a custom MATLAB (MathWorks, Natick, MA, USA)-based software (Fricker, 2016). For experiments with dark/light/dark transitions, protonema and gametophores of *TKTP-roGFP2*-expressing transgenic *P. patens* lines WT #20, Δ*grxc5* #17 and Δ*grxc5* #21 cultured in liquid medium were dark-adapted for at least 45 min. Subsequently, roGFP2 fluorescence was first imaged for 1 min in the dark (without pre-screening), then during illumination from an external light source with c. 100 µmol photons $m^{-2}s^{-1}$ from a 90° angle for 5 min (every 30 s), followed by a second period of continued imaging in the dark (Müller-Schüssele et al., 2020).

In vivo plate-reader based fluorometry

Ratiometric time-course measurements for roGFP2 were conducted using a CLARIOstar® Plus plate reader (BMG Labtech). During *in vivo* time series, roGFP2 signal was detected using a sequential filter-based excitation of 400-10 nm and 482-16 nm, while emission was detected at 530-40 nm. The degree of oxidation of roGFP2 (OxD) was calculated as described in Aller et al. (2013). Protonema culture of *P. patens* expressing *TKTP-roGFP2* was dispersed and transferred to fresh KNOP-ME pH 5.8 media one week prior to measurements. 200 µl of protonema culture were pipetted with a wide cut pipette tip into wells of a 96-well plate. Cultivation media was taken up after the moss settled to the bottom of the plate and substituted by 200 µl of imaging buffer (10 mM MES, 5 mM KCl, 10 mM $CaCl_2$, 10 mM $MgCl_2$ pH 5.8) (Wagner et al., 2019). To conduct an *in vivo* sensor calibration, the 200 µl imaging buffer were removed with a 100 µl tip and substituted with the same volume of imaging buffer containing either 10 mM H_2O_2 or 5 mM DPS (2,2'-dipyridyl disulfide) for complete oxidation, and 10 mM dithiothreitol (DTT) for complete reduction.

For H_2O_2 recovery experiments, H_2O_2 in concentrations ranging from 1-10 mM were added manually to the wells. After 30 min in the respective H_2O_2 in concentration, buffer was exchanged to imaging buffer to follow roGFP2 re-reduction. For H_2O_2 oxidation rate experiments the plate reader was used in "well mode" with a cycle time of 1.55 s. 200 µl of one-week-old protonema culture expressing *TKTP-roGFP2* was transferred into a 96-well plate and pre-reduced using 10 mM DTT in imaging buffer. DTT was removed and substituted with 160 µl imaging buffer. After 60 s H_2O_2 was automatically injected by the plate reader to a final concentration of 2 mM.

Excitation scans were performed on *P. patens* protonema tissue expressing *TKTP-roGFP2*: 100 µl of one-week-old liquid culture was transferred into a 96-well plate and either treated for 30 min with 10 mM DTT, 5 mM DPS or imaging buffer. Wells were excited at 390-490 nm using a monochromator while emission was collected at 535-16 nm. Intensities of excitation spectra were normalized to the intensity of the isosbestic point of roGFP2 at c. 425 nm.

CO_2 exchange measurements

CO_2 exchange measurements were performed with the GFS-3000 (Heinz Walz GmbH, Effeltrich, Germany). For each measurement, WT, Δ*grxc5* #54, and Δ*grxc5* #249 protonema cultures were cultivated in parallel to a similar density in liquid medium. Three days after sub-culturing, 5 ml of each culture were applied onto a nylon membrane filter with a diameter of 35 mm, placed within a miniature petri dish (Ø 42 mm). Any excess liquid was removed using a 1000 µl pipette tip. CO_2 uptake was recorded for 7.5 min in light (75 µmol photons m^{-2} s^{-1}), followed by 7.5-minute in darkness. These measurements were performed consistently at a humidity level of 98% and a temperature of 22 °C, with this cycle repeated three times per biological replicate to ensure reliability. To establish a baseline measurement, a nylon

membrane filter wetted with KNOP-ME medium was used as a blank (zero point; ZP) before each measurement. The recorded ZP value was subtracted from each measurement point (MP). In **Fig. 6**, data from the last 2.5 min of the first dark cycle to the third dark cycle (dark-light-dark transition) from five biological replicates from different weeks were plotted.

SDS-PAGE and Western blotting

Protein extraction based on chloroform-methanol precipitation was performed according to (Wessel and Flügge, 1984; Mueller et al., 2014) on frozen and pulverized plant material using the TissueLyser II (Qiagen). 100 µl lysis buffer (7.5 M urea, 2.5 M thiourea, 12.5% (v/v) glycerol, 62.5 mM Tris-HCl pH 8, 0.1% (v/v) Sigma plant protease inhibitor cocktail (P9599)) was added per 10 mg pulverized plant material. Additionally, protein thiol groups were blocked by a final concentration of freshly balanced 20 mM *N*-ethylmaleimide (NEM, Sigma 128-53-0) directly added to the lysis buffer. Protein pellets were dissolved in 50-100 µl protein resuspension buffer (50 mM Tris-HCl, 8 M urea, pH 7.5-8). SDS-PAGE samples were prepared by mixing the proteins sample with 1x non-reducing Laemmli buffer (2% (w/v) SDS, 50 mM Tris-HCl pH 6.8, 0.002% (w/v) bromophenol blue, 10% (v/v) glycerol), and size-separated using 10% Mini-PROTEAN® precast gels (Bio-Rad) (SDS-running buffer 25 mM Tris-HCl pH 8.3, 192 mM glycine, 0.1% (w/v) SDS) according to the manufacturer's instructions, using 5 µl PageRuler™ Prestained Protein Ladder (ThermoFisher) as marker. Equal loading was confirmed by staining for >1 h in PageBlue™ protein staining solution (ThermoFisher).
Proteins were transferred to a PVDF membrane (Immobilon-P, Millipore Corporation, Billerica, MA, USA) via semi-dry Western blotting. The membrane containing the proteins was blocked in 5% (w/v) milk powder dissolved in TBS-T buffer (20 mM Tris-HCl pH 7.6, 137 mM NaCl, and 0.1% (v/v) Tween20) for 1 h at 25 °C or overnight at 4 °C before labelling with the primary antibody (α-GSH, ThermoFisher, MA1-7620, 1:1000 in 2.5% (w/v) milk powder dissolved in TBS-T). Membranes were washed three times with TBS-T for 5 min and incubated for 1 h in the secondary antibody (Goat anti-Mouse, Agrisera, AS11 1772, 1:2500 in TBS). For immunodetection the Agrisera ECL kit (Super Bright, AS16 ECL-SN) was used according to the recommendations of the supplier. Western blots were imaged using the INTAS ECL ChemoStar imaging system (Intas).

Results

PpGRXC5 is a class I GRX with (de)glutathionylation activity

First, we determined PpGRXC5 (de)glutathionylation activity and kinetic parameters *in vitro*, by cloning and purifying PpGRXC5 (removing the N-terminal targeting sequence, starting with Ala120). We characterized K_m^{app} and k_{cat}^{app} of PpGRXC5 using the hydroxyethyl disulfide (HED)-assay. PpGRXC5 was able to very efficiently catalyse the GSH-dependent reduction of

HED (Begas et al., 2015) with catalytic efficiencies (k_{cat}^{app}/K_m^{app}) of 1.0 x10^5 $M^{-1}s^{-1}$ and 2.8 x10^4 $M^{-1}s^{-1}$ when HED and GSH were used a variable substrate, respectively (**Fig. 2A**).These catalytic efficiency constants are in a comparable order of magnitude with class I GRX7 from *S. cerevisiae* , *Plasmodium falciparum* (Begas et al., 2017) and class I GRXs from the green lineage, such as *Chlamydomonas reinhardtii* GRX1 (Zaffagnini et al., 2008), poplar PtGRXS12 (Couturier et al., 2009; Zaffagnini et al., 2012a) and AtGRXC5 (Couturier et al., 2011).

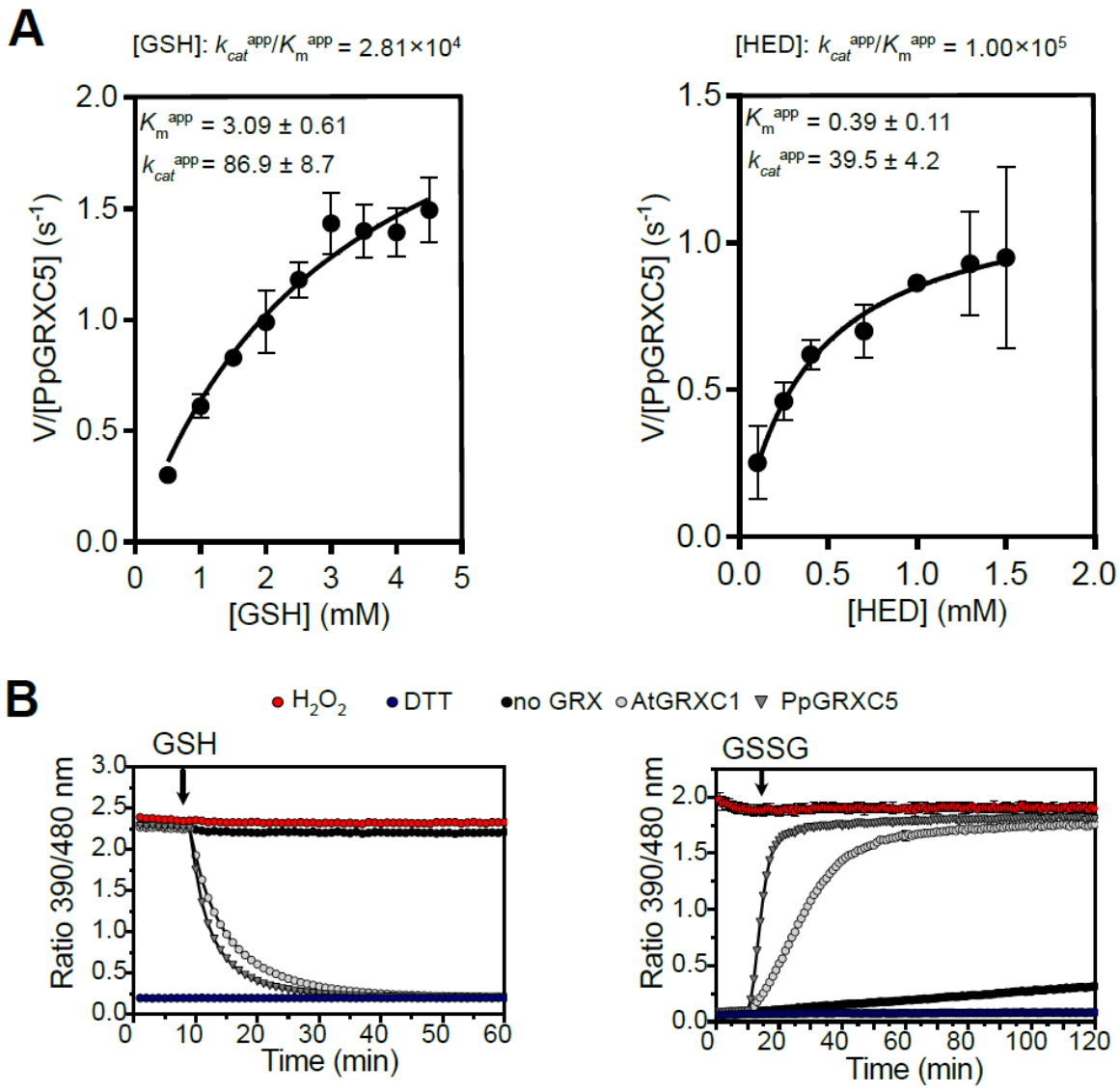

Figure 2: Catalytic activity of PpGRXC5 *in vitro*

(A) HED assays: PpGRXC5 [30 nM] was added to a cuvette containing GSH [0.5-4 mM], HED [0.3-1.5 mM], NADPH [200 µM], GR [6 µg/ml] in 100 mM Tris-HCl, 1 mM EDTA, pH 7.9. The decrease in absorbance at 340 nm was followed for 1 min (shown are means± SDs, n = 4). Varying concentration of GSH [0.5-4 mM] and a constant HED concentration of 0.7 mM was used to determine GSH-dependent kinetics (left panel)**.** Varying concentrations of HED [0.3-1.5 mM] and a concentration of 1 mM GSH was used to determine HED-dependent kinetics (right panel). Apparent K_m (K_m^{app}) is depicted in mM, apparent k_{cat} (k_{cat}^{app}) in s^{-1} and the rate constant (k_{cat}^{app}/K_m^{app}) in $M^{-1}s^{-1}$. Non-linear regression was fitted using Prism 9 (GraphPad). **(B)** roGFP2 reduction assay (left panel): 1 µM of PpGRXC5 or 1 µM AtGRXC1 were incubated with 1 µM of oxidized roGFP2 in 100 mM KPE, pH 7.4. Arrow indicates the time point of addition of 2 mM GSH; n = 3 ± SDs. roGFP2 oxidation assay (right panel): 1 µM of PpGRXC5 or 1 µM AtGRXC1 were incubated with 1 µM of pre-reduced roGFP2. Arrows indicate the time point of addition of 40 µM GSSG. As oxidation and reduction controls (calibration), 1 µM of roGFP2 was treated with 10 mM of DTT or 10 mM H_2O_2; n = 3 ± SDs.

As class I GRXs show oxidoreductase activity on disulfides that are formed and released via a *S*-glutathionylation intermediate (Lillig et al., 2008; Deponte, 2022), redox-sensitive GFP2 is a suitable target protein for *in vitro* assays, providing a direct fluorescent read-out for disulfide redox state (Meyer et al., 2007; Gutscher et al., 2008; Schwarzländer et al., 2008; Meyer and Dick, 2010). Hence, we tested PpGRXC5 oxidizing and reducing activity on recombinant roGFP2, in a direct comparison with the previously characterized AtGRXC1 (Trnka et al., 2020) **(Fig. 2B)**. In the *in vitro* roGFP2 reduction and oxidation assays PpGRXC5 was able to reduce and oxidise roGFP2 kinetically faster than AtGRXC1, confirming high activity in the reductive half-reaction and additionally showing high activity in the oxidative half-reaction of thiol-disulfide oxidoreductase function. Thus, PpGRXC5 is a typical class I GRX that shows efficient (de)glutathionylation as well as thiol-disulfide oxidoreductase activities.

The single stromal class I GRX PpGRXC5 is dispensable and not a main cause for the dwarfism in Δ*gr1* mutants

To generate null mutants of PpGRXC5 in *P. patens* we used homologous recombination **(Fig. 3A)**. We confirmed several independent transgenic lines of which we used the null mutants Δ*grxc5*#54 and Δ*grxc5*#249 **(Fig. S1)** for further experimentation. Growth under standard conditions was comparable to the wild-type **(Fig. 3B)**, which is in contrast to the previously characterised dwarfed *P. patens* glutathione reductase knockout lines (Δ*gr1*) that exhibit a less reducing stromal steady-state E_{GSH} (Müller-Schüssele et al., 2020). As PpGRXC5 can contribute to plastid GSSG generation or mediate *S*-glutathionylation **(Fig. 1)**, we additionally tested whether the defects observed in Δ*gr1* were dependent on GRXC5 activity. To this end, we generated Δ*gr1*/Δ*grxc5* double knock-outs by transforming the Pp*GR1* knock-out construct (Müller-Schüssele et al., 2020) into protoplasts of Δ*grxc5*#54 and confirmed the correct integration and absence of transcript for *GR1* **(Fig. S1)**. Lack of GRXC5 did not rescue the Δ*gr1* phenotype, as Δ*gr1*/Δ*grxc5* mutant lines were dwarfed **(Fig. 3B)**. Quantification of growth revealed a trend for increased fresh weight of Δ*gr1*/Δ*grxc5* compared to Δ*gr1*, that was not statistically significant **(Fig. S2)**. In addition, Δ*gr1*/Δ*grxc5* showed the same sensitivity to oxidative stress as Δ*gr1* (H_2O_2 treatment, **Fig. 3C)**. Thus, neither GSSG generation by PpGRXC5 nor an involvement in a putative toxic *S*-glutathionylation is contributing to the major defects observed in Δ*gr1* lines.

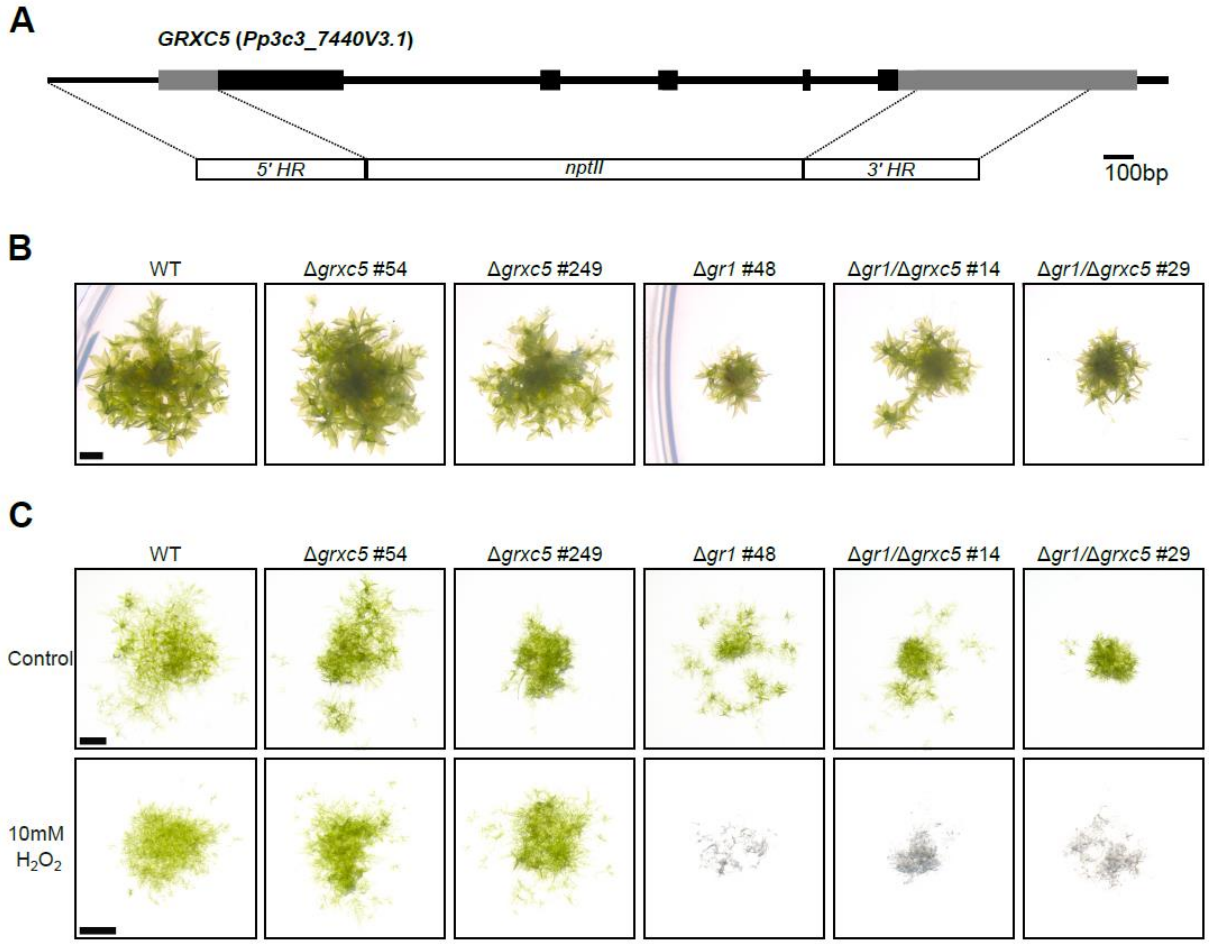

Figure 3: Phenotype of Δ*grxc5,* Δ*gr1* and Δ*gr1*/Δ*grxc5* plants

(A) Schematic overview of the Pp*GRXC5* gene structure and knock-out construct; exons = boxes; UTRs (untranslated regions) light grey, coding sequence black; HR, homologous regions; *nptII*, neomycin phosphotransferase resistance cassette. **(B)** *P. patens* grown on KNOP-ME pH 5.8 agar plates in 100 µmol photons $m^{-2}s^{-1}$ (16 h light, 8 h dark) for four weeks, scale bar = 1mm. Row represent colonies grown on the same plate. **(C)** Protonema culture spotting assay on KNOP-ME plates after incubating with 10 mM of H_2O_2 for 15 minutes as oxidative challenge. A 20 µl aliquot of protonema culture was placed on a KNOP-ME agar plate and grown under 60 µmol photons $m^{-2}s^{-1}$ (16 hours light, 8 hours dark) for 7 days. Control cultures were treated equally except for addition of H_2O_2. Images were taken after 7 days of recovery. Scale bar: 1 mm.

To further test for altered stress resilience or growth defects in Δ*grxc5* lines, we exposed plants to low light, fluctuating low light/high light and heat, but did not identify any morphological differences to WT **(Fig. S3)**. To test for differences in photosynthetic light reactions, we determined light-induction and relaxation kinetics, calculating non-photochemical quenching (NPQ) under control conditions and after exposure to high light (450 µmol photons m^{-2} s^{-1}). Δ*gr1* plants showed increased non-photochemical quenching (NPQ) combined with retarded relaxation kinetics consistent with a previous report (Müller-Schüssele et al., 2020), while Δ*grxc5* lines did not show any significantly different response in NPQ induction or relaxation **(Fig. S4)**. Our results confirm that neither the growth defect nor the sensitivity to high light of Δ*gr1* plants is detectable in Δ*grxc5* plants, indicating that the negative effects of the less

negative E_{GSH} in Δ*gr1* plants are not mediated via GRXC5. Instead, Δ*grxc5* plants showed WT-like growth in all long-term stress assays.

Lack of class I GRX leads to distinct roGFP2 oxidation state and changed reduction kinetics after oxidative challenge in the stroma

As we did not identify phenotypical deviations of Δ*grxc5* lines from WT macroscopically, we sought to investigate stromal redox dynamics *in vivo* by introducing a genetically encoded biosensor. Redox-sensitive GFP2 (roGFP2) specifically equilibrates with the steady-state E_{GSH} of the local subcellular compartment (Meyer et al., 2007; Schwarzländer et al., 2008). As this equilibration is catalysed by class I GRX, human GRX1 (hGrx1) fused to roGFP2 (Grx1-roGFP2) is the standard probe used, to guarantee independence from local endogenous GRX activities (Gutscher et al., 2008). Since it was our aim to measure the endogenous GRX activity we exploited the requirement of GRX-mediated equilibration and targeted roGFP2 without fused hGRX1 to the plastid stroma of WT and Δ*grxc5#54* genetic backgrounds. We generated a construct for expression of roGFP2 fused to the transketolase targeting peptide (TKTP) (Schwarzländer et al., 2008; Speiser et al., 2018)), constitutively driven by the Pp*Actin5* promoter, targeting roGFP2 to the plastid stroma. Exclusive targeting of roGFP2 to plastids in stable transgenic lines was confirmed microscopically **(Fig. S5)** and sensor lines for each background were characterised and selected for further analyses (*TKTP-roGFP2* in Δ*grxc5#54* lines #17 and #21; *TKTP-roGFP2* in WT #20).

Sensor responsiveness to oxidation/reduction *in vivo* was confirmed via addition of either 10 mM DTT (reductant) or 5 mM DPS (2,2'-dipyridyl disulfide, thiol-specific oxidant) to moss protonema. Using a fluorescence plate-reader, excitation spectra for roGFP2 fluorescence were recorded **(Fig. 4A)**, revealing a comparable dynamic range (between 2.0 and 2.2 (405/488)) of the sensor response in WT and Δ*grxc5* background. In comparison to TKTP-roGFP2 WT#20, the physiological (untreated, Phys.) spectra of Δ*grxc5* sensor lines revealed lower excitation above the isosbestic point (c. 425 nm) and higher excitation below 425 nm, showing increased oxidation of roGFP2 of c. 20% (calculated for 405/488 nm). We additionally quantified this oxidation by ratiometric analysis of confocal images of the respective lines and found an increase in median 405/488 ratio of 1.64 ± 0.59 in Δ*grxc5#17,* 1.54 ± 0.40 in Δ*grxc5#21* compared to 1.15 ± 0.38 in WT#20 **(Fig. 4B)**. Taking into account sensor calibration (*i.e.*, ratio values for complete reduction and oxidation *in vivo*), these values support a by c. 20% higher degree of oxidation (OxD) on stromal roGFP2, compared to WT, in untreated cells.

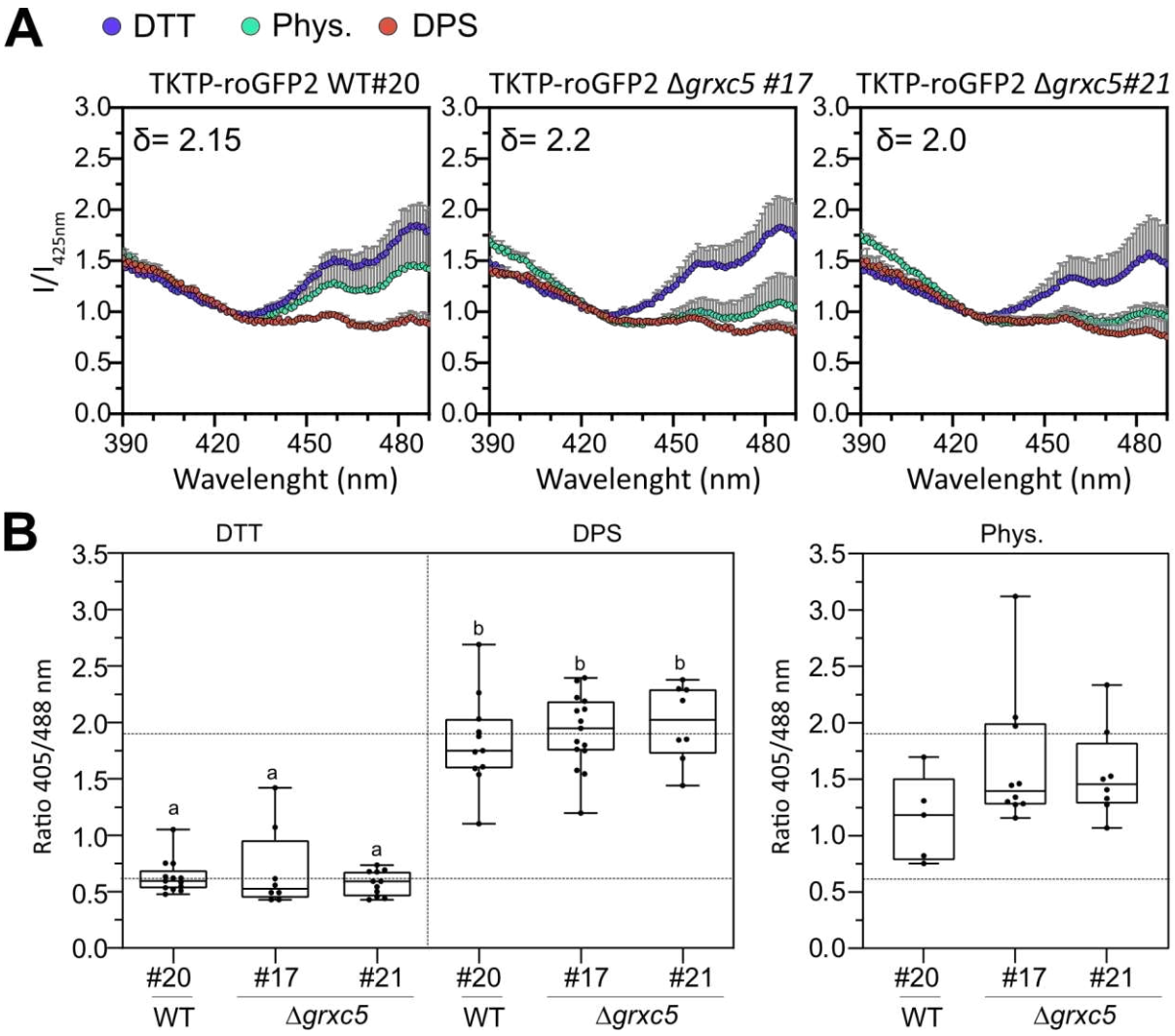

Figure 4: Redox state of stroma-targeted roGFP2 in WT and Δ*grxc5*

(A) *In vivo* excitation spectra: protonema cultures of *P. patens* were not treated (Phys.) or treated for 30 min with 10 mM DTT or 5 mM DPS. Fluorescence was excited from 390 to 490 nm while emission was collected at 535-16 nm in a plate-reader based setup. Intensities were normalized to the intensity of the isosbestic point of roGFP2 (425 nm); n=3, mean + SD. Delta depicts the dynamic range (405/488 nm) for each line. **(B)** Left panel: Image-based sensor calibration of TKTP-roGFP2 in *P. patens* with 10 mM DTT or 5 mM DPS incubated for at least 20 min before imaging with the CLSM (ex. 405, 488 nm; em. 508-535 nm); n>7, box blots: line=median and whiskers=min/max values; two-way ANOVA and Tukey's multiple comparison test was conducted ($p<0.0001$), different lowercase letters indicate significant difference, dynamic range c. 3.2. Right panel: image-based analysis of steady state sensor ratio (405/488 nm) under physiological conditions: *P. patens* protonema/gametophore culture was pre-incubated in the dark for 30 min before imaging with the CLSM (ex. 405, 488 nm; em. 508-535 nm); n=5-10 pictures, box blots: line=median and whiskers=min/max values, one-way ANOVA and Tukey's HSD test (ratio~genetic background, p=0,08); horizontal lines: 0% and 100% oxidation based on mean DTT and mean DPS values, according to sensor calibration, see left panel.

As higher OxD values for roGFP2 are interpreted as a less negative stromal E_{GSH}, at least in the presence of GRX activity, we additionally quantified total GSH levels by HPLC from five biological replicate samples of protonema and found a trend for an increase in total glutathione in Δ*grxc5*#54 (p=0.15) and a significant increase in total glutathione in Δ*grxc5*#249 (p=0.0006), compared to WT (one-way ANOVA, Tukey's multiple comparison) **(Fig. S6)**. These analyses suggest that loss of PpGRXC5 causes a higher steady state OxD of roGFP2 in the stroma, as well as a trend to increased GSH levels.

As long-time exposure to various stresses did not reveal any defects in Δ*grxc5* lines, we simulated a pulse of oxidative stress to generate a temporary oxidation and compared the subsequent recovery. We exposed moss protonema to 10 mM H_2O_2, which causes complete oxidation of roGFP2. After removal of H_2O_2, we monitored the recovery kinetics of roGFP2 reduction state. While the WT background showed a fast recovery almost immediately after removal of H_2O_2, Δ*grxc5* null mutants showed slower, approximately linear recovery of roGFP2 redox state **(Fig. 5A)**. Using lower H_2O_2 concentrations in a 1-5 mM range, fast recovery was already observable during the presence of exogenously added oxidant in the WT background while Δ*grxc5* null mutants consistently showed slower, approximately linear recovery from oxidative stress **(Fig. S7)**. To additionally monitor oxidation kinetics of the roGFP2 disulfide, we pre-reduced moss protonema and subsequently used injection of H_2O_2 combined with 1.5 s measuring intervals. We found that oxidation of roGFP2 in Δ*grxc5* stroma proceeded equally fast or slightly faster **(Fig. 5B)**. Thus, disulfide formation in response to severe oxidative stress is fast in Δ*grxc5* null mutants while stromal GSH-dependent disulfide reduction is slow and almost linear.

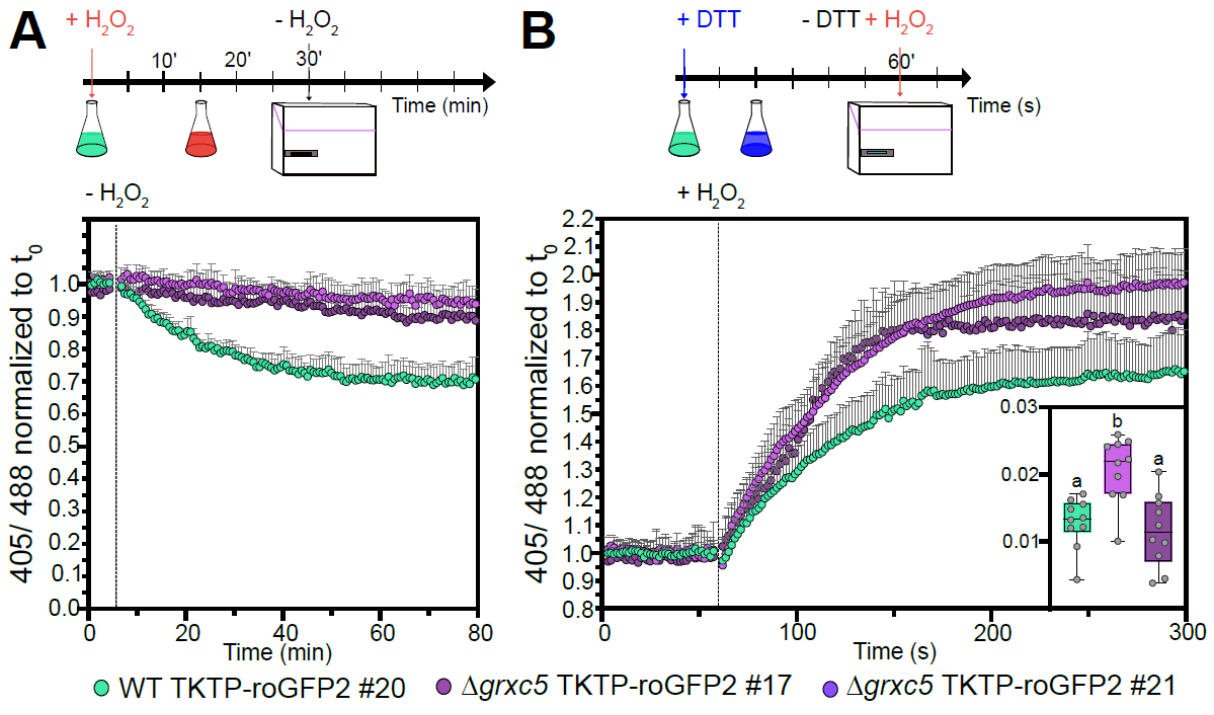

Figure 5: *In vivo* kinetics of stromal roGFP2 in response to oxidative challenge

(A) Protonema culture expressing *TKTP-roGFP2* was treated with 10 mM H_2O_2 for 30 min and H_2O_2 subsequently removed and exchanged with imaging buffer to monitor recovery from oxidative challenge. 405/488 nm ratio of n=6 biological replicates was normalized to t_0, graph depicts mean+SD. A two-way ANOVA with Tukey's multiple comparison test was conducted for each time point revealing significant differences in roGFP2 kinetics between WT and both Δgrxc5 #17 and Δgrxc5#21 starting from 11 min after peroxide removal ($p < 0.001$, n=6). **(B)** *In vivo* oxidation rates after injection of H_2O_2 (final concentration = 2 mM) and monitoring of oxidation rate every 1.55 s. Protonema samples were pre-reduced using 10 mM DTT. Shown are the mean + SD, n=10. Slope (inset, $\Delta R/\Delta t$) was calculated for the first 10 s after injection (eight data points). Box plot whiskers depict min and max values with the horizontal line indicating the median. One-way ANOVA with Tukey's multiple comparison test was conducted to test for significant difference ($p<0.027$).

Linking *S*-glutathionylation levels to oxidative challenge and GRX activities

Using roGFP2 enabled us to observe disulfide formation and reduction kinetics in the absence of a class I GRX under different environmental conditions. However, disulfides would only be formed in response to *S*-glutathionylation if a second cysteine is present in a suitable distance to reduce the mixed disulfide, forming an intramolecular disulfide and concomitant release of GSH **(Fig. 1)**. While this is the case for roGFP2, many *in vivo* targets of class I GRXs may remain in a *S*-glutathionylated state (Zaffagnini et al., 2012b; Müller-Schüssele et al., 2021a). Hence, we investigated if total protein *S*-glutathionylation levels are altered in Δ*grxc5* null mutants, using Western blotting with an anti-GSH antibody **(Fig. 6)**. As a control, we incubated *in vitro* purified roGFP2 mutant lacking the resolving Cys204 (roGFP2C204S) (Trnka et al., 2020) with 10 mM H_2O_2 in the presence of 2 mM GSH, inducing *S*-glutathionylation. Protein extracts from non-stressed and stressed WT and Δ*grxc5* plants both showed equally increased signal after immunodetection of protein-bound GSH, starting from a similar level. Increase of protein-bound GSH was consistent and independent of presence of GRXC5 after oxidative challenge **(Fig. S8)**.

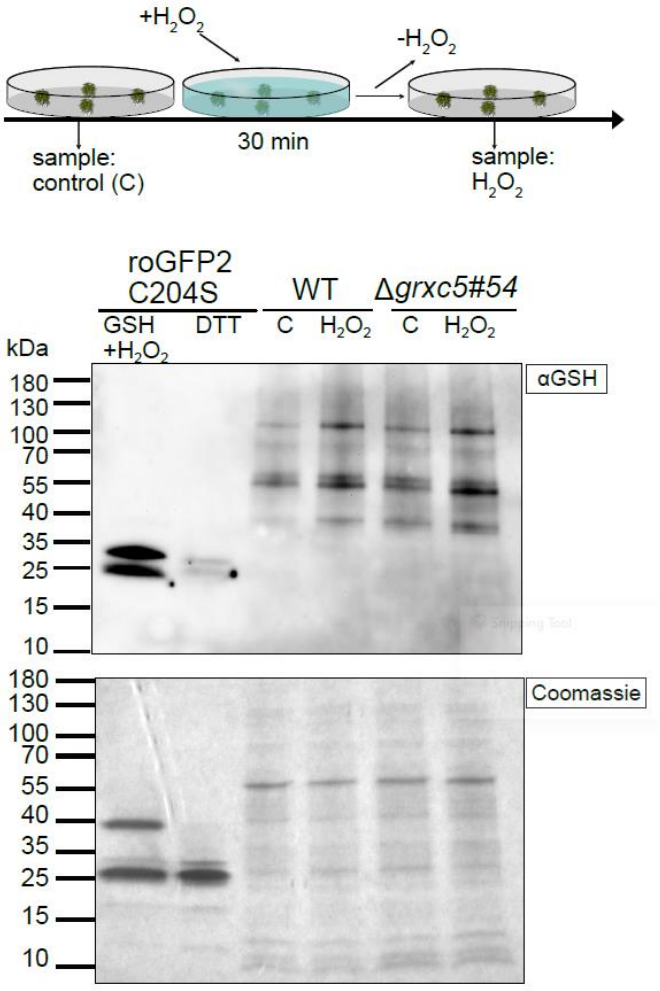

Figure 6 Total protein-bound glutathione after oxidative challenge

(A) Schematic overview of the experimental set-up and sampling. **(B)** Immunoblot using α-GSH (ThermoFisher). Total protein extracts from *P. patens* WT and Δ*grxc5*#54 gametophore tissue either non-treated ('C') or treated with 10 mM H_2O_2 for 30 min ('H_2O_2') (see panel A); cysteine oxidation was blocked with 20 mM NEM (*N*-ethyl maleimide) in the lysis buffer. As loading control, 10 µg total protein was loaded onto a 4-20% gradient non-reducing SDS-PAGE lower panel). As control for antibody specificity, purified roGFP2C204S (10 µM) was treated with 10 mM H_2O_2 in the presence of 2 mM of GSH for 30 min (positive control, glutathionylated roGFP2C204S) or treated with 10 mM DTT (negative control, no glutathionylated roGFP2C204S), and 12 µl loaded per lane.

Stromal GSH-dependent redox kinetics are altered in dark/light/dark transitions, without an effect on carbon fixation

As stromal Grx1-roGFP2 showed a previously unknown light/dark transition-dependent E_{GSH} dynamics in WT (Müller-Schüssele et al., 2020), we next assessed stromal roGFP2 redox dynamics in Δ*grxc5* null mutants using both a plate-reader based setup **(Fig. 7A)** and a confocal microscopy-based setup (Müller-Schüssele et al., 2020) **(Fig. 7B)**. We found that light/dark transition-dependent dynamics of stromal roGFP2 oxidation state were also observable using roGFP2 without fused Grx1 in WT background: a sudden light to dark transition leads to rapid sensor oxidation, followed by a recovery phase. In contrast, light/dark dependent roGFP2 redox changes were completely absent in Δ*grxc5* null mutants. Responsiveness of the roGFP2 probe was confirmed after light/dark treatment by calibration **(Fig. 7A)**, demonstrating that roGFP2 redox state in Δ*grxc5* was well inside dynamic range of roGFP2. As a complementary approach, we used a CLSM-based setup where we were also able to follow roGFP2 redox state in the light and confirmed absence of dark/light/dark transition-dependent roGFP2 redox dynamics in Δ*grxc5* **(Fig. 7B)**.

As our results suggest potential differences in glutathione-dependent redox dynamics in the chloroplast stroma, we assessed cross-talk to the TRX system by quantifying CO_2 release and assimilation from protonema in a dark/light/dark transition **(Fig. 7C)**. Our analysis did not find any significant differences in either CO_2 release in the dark, nor in CO_2 uptake in the light, suggesting overall unaltered redox-regulation of the CBB cycle enzymes in Δ*grxc5* lines, compared to WT. Thus, fast responses of the roGFP2 redox state to light/dark dependent E_{GSH} dynamics are absent in Δ*grxc5* plants, while regulation of carbon fixation was unaltered under the tested conditions.

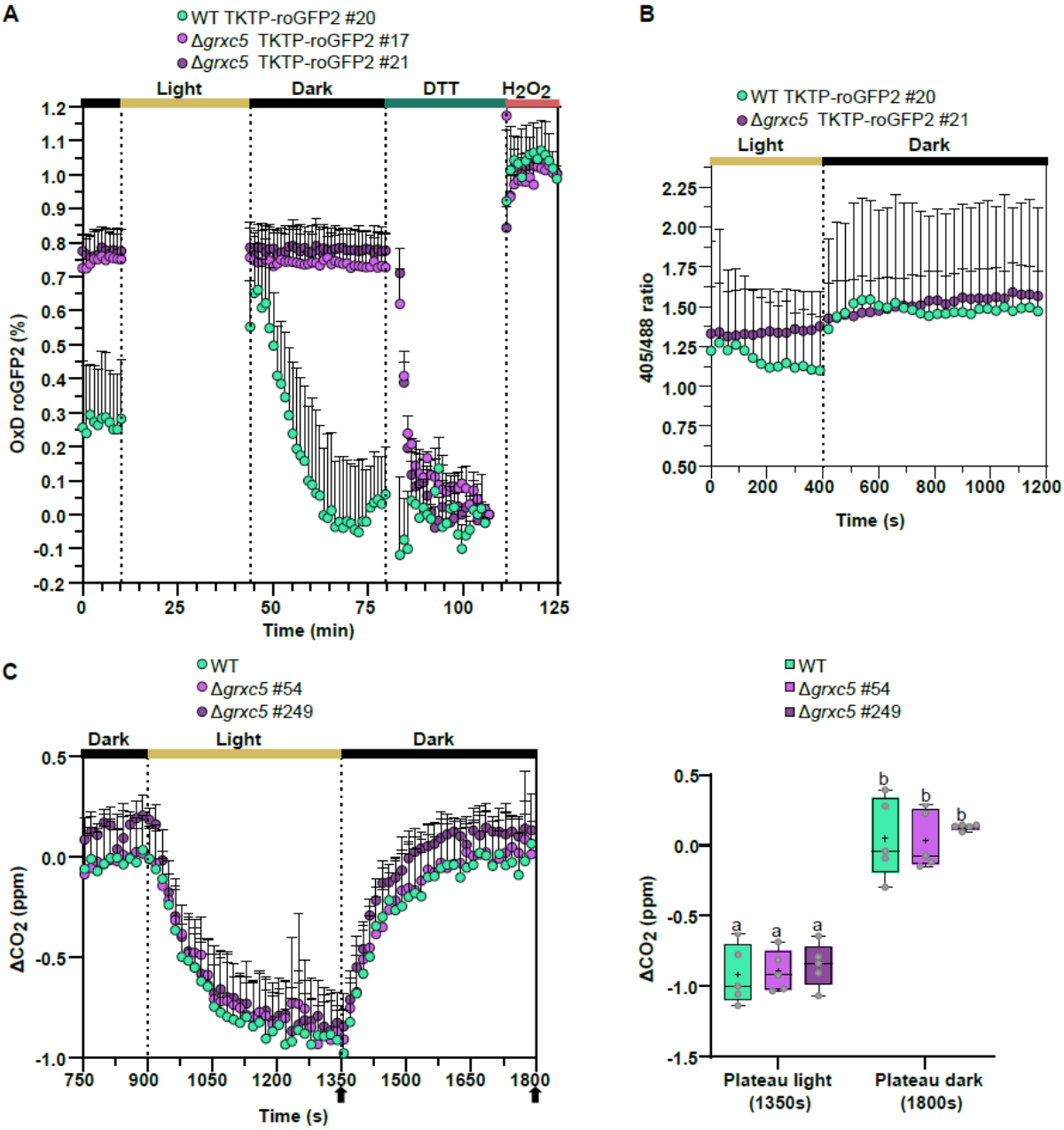

Figure 7: Light-dependent roGFP2 dynamics and CO_2 assimilation during dark-light-dark transitions in protonema culture of Δ*grxc5* and WT

(A) Reduction/oxidation dynamics in dark/light/dark transitions. In a 96-well plate with 200 µl of protonema culture from *P. patens*, initial fluorescence was measured after 30 min dark incubation using a plate reader-based setup. Subsequently, the plate was illuminated for 30 minutes to an intensity of ~200 µmol photons $m^{-2}s^{-1}$ using external LED illumination. After dark/light/dark transition, each well was calibrated by first replacing the buffer with 10 mM DTT and then10 mM H_2O_2. OxD = degree of oxidation, shown are the mean (+SD) of n=3. **(B)** Image-based analysis of oxidation/reduction dynamics of TKTP-roGFP2 in *P. patens* gametophores and protonema tissue grown in liquid culture. CLSM time series of dark-adapted samples: 1 min in the dark, illumination by external light source for 5 min (100 µmol photons $m^{-2}s^{-1}$), followed by dark incubation. Images were taken every 30 seconds for 20 minutes; shown is the mean + SD of n=7-8. **(C)** Left panel: changes in CO_2 partial pressure during dark/light/dark transitions in protonema culture of Δ*grxc5* lines and WT using a 7.5 min light and 7.5 min dark cycle (98% humidity, 500 ppm CO_2, 22 °C, and 75 µmol photons $m^{-2}s^{-1}$). The absolute changes in CO_2 levels were measured after zero-point (ZP) subtraction (nylon membrane filter wetted with KNOP-ME as ZP). Right panel: Changes in CO_2 partial pressure after reaching plateau values during the light and dark phases, respectively (indicated by arrows in left panel). One-way ANOVA and Tukey's multiple comparison to assess significant differences between Δ*grxc5* lines and WT at the end of the light cycle (1350s) and the end of the dark cycle (1800s): p=0.99. Boxes display the 25-75 percentiles, with the minimum and maximum values indicated by the whiskers, and the median marked by the horizontal line (n=5).

Discussion

Glutathione as an electron donor in the plastid stroma

Thiol redox states depend on their reaction kinetics with different small molecules or protein reductants and oxidants, including thiols in a suitable distance for disulfide formation. Different thiol/oxidised thiol redox couples can be in thermodynamic equilibrium after incubation in the range of minutes to hours, whereas enzymatically catalysed equilibration takes place in the range of seconds to minutes. GRX-catalysed redox equilibration depends on GSH as electron donor. We determined the enzyme kinetics of PpGRXC5 (YCPYC active site) *in vitro* and found high deglutathionylation activity (HED assays) as well as thiol-disulfide oxidoreductase activity (roGFP2 *in vitro* assays). The apparent second-order rate constant(s) (k_{cat}^{app}/K_m^{app}) for PpGRXC5-catalyzed reactions (HED assay) was similar to AtGRXC1 (YCGYC active site) (Riondet et al., 2012) or AtGRXC5 (WCSYC active site) (Couturier et al., 2011), showing that GRXC5 is an evolutionary conserved redoxin (Müller-Schüssele et al., 2021a) with a typical class I GRX functionality as GSH-dependent (de)glutathionylation and thiol/disulfide oxidoreductase activity.

Disulfides can be characterized by their midpoint potential, *i.e.*, the redox potential at which 50% of the molecules are reduced and 50% oxidized. The disulfide formed by the genetically encoded biosensor roGFP2 is well-characterised, with a consensus midpoint potential of -280 mV (pH 7), and enzymatically catalysed by GRX in dependence on E_{GSH} ((Dooley et al., 2004; Meyer et al., 2007; Gutscher et al., 2008; reviewed in Meyer and Dick (2010); Schwarzländer et al. (2016); Müller-Schüssele et al. (2021b)). We targeted this redox sensor protein to the plastid stroma, without the fusion to a GRX, to track local GSH-coupled redox dynamics in the model moss *P. patens*. In the stroma of WT plants, roGFP2 redox state indicated a steady-state stromal E_{GSH} of c. -312 mV (pH 8), consistent with the -311 mV (pH 8) measured using Grx1-roGFP2 in WT background of *P. patens* plastid stroma (Müller-Schüssele et al., 2020). A similar physiological steady-state stromal E_{GSH} in the dark-adapted state of WT using either roGFP2 or Grx1-roGFP2 confirms similar functionality of roGFP2 in WT stroma, without fused hGrx1. Compared to WT, we detected an increased 405/488 nm ratio and corresponding increased roGFP2 degree of oxidation (OxD) of c. 20% in the stroma of Δ*grxc5* lines. In addition, we found a trend for increased total GSH content, which would according to the Nernst equation suggest more negative E_{GSH}, although HPLC measurements do not allow for subcellular resolution. A shift of roGFP2 thiol/disulfide redox state to more oxidized values usually reveals an oxidative shift in E_{GSH}, as roGFP2 specificity for the glutathione/GRX system was tested *in vitro* and *in vivo* (Meyer et al., 2007; Begas et al., 2017; Trnka et al., 2020; Schlößer et al., 2023). Thus, inefficient reduction of GSSG caused by absence of glutathione reductase (GR) leads to an increase of OxD_{roGFP2} in the same subcellular compartment (Marty et al., 2009; Marty et al., 2019; Müller-Schüssele et al., 2020).

In Δ*gr1* lines, a shift of c. 44% in OxD_{roGFP2} was measured using stroma-targeted Grx1-roGFP2 which reports an oxidative stromal E_{GSH} shift of c. 33 mV (Müller-Schüssele et al., 2020). In theory, the measured shift in roGFP2 redox status in the Δ*grxc5* lines may either indicate altered E_{GSH}, *i.e.*, local decrease in GSH and/or local increased GSSG concentration, or inefficient equilibration between E_{GSH} and roGFP2 (or a combination of both). The following argument supports an oxidative shift in OxD_{roGFP2} in the Δ*grxc5* stroma independent of a change in local E_{GSH}: (1) GR is still present in the stroma of Δ*grxc5*, safeguarding the highly reducing stromal E_{GSH}. (2) *In vivo* stromal roGFP2 reduction rates after oxidative challenge (**Fig. 5A**) are similar (i.e. in the range of minutes to hours) to thermodynamically driven *in vitro* reduction rates based on highly negative E_{GSH}, but lacking addition of GRX (**Fig. 2B**, (Meyer et al., 2007)). Thus, without class I GRX present, a shifted OxD_{roGFP2} likely originates from a decreased glutathione-dependent reduction rate of the roGFP2 disulfide, never reaching thermodynamic equilibrium with E_{GSH}. Instead the interaction with other redox couples becomes apparent in the form of the oxidation (i.e. unchanged oxidation rates), resulting in an OxD_{roGFP2} steady state further away from thermodynamic equilibrium with glutathione as electron donor (schematic model **Fig. 8**). After oxidative challenge, lacking GRXC5 activity leads to slow recovery rates from higher thiol oxidation levels (**Fig. 8**). Thus, Δ*grxc5* and Δ*gr1* mutants both show altered OxD_{roGFP2} *in vivo*, but through different mechanisms, *i.e.*, lacking reduction of GSSG *vs.* kinetic uncoupling between E_{GSH} and disulfide redox state. Our data show that fast enzymatically catalysed equilibration of roGFP2 redox state with the highly reduced glutathione pool is not complemented by other redox systems present in the stroma and confirm PpGRXC5 as the sole stroma-targeted class I GRX in *P. patens*.

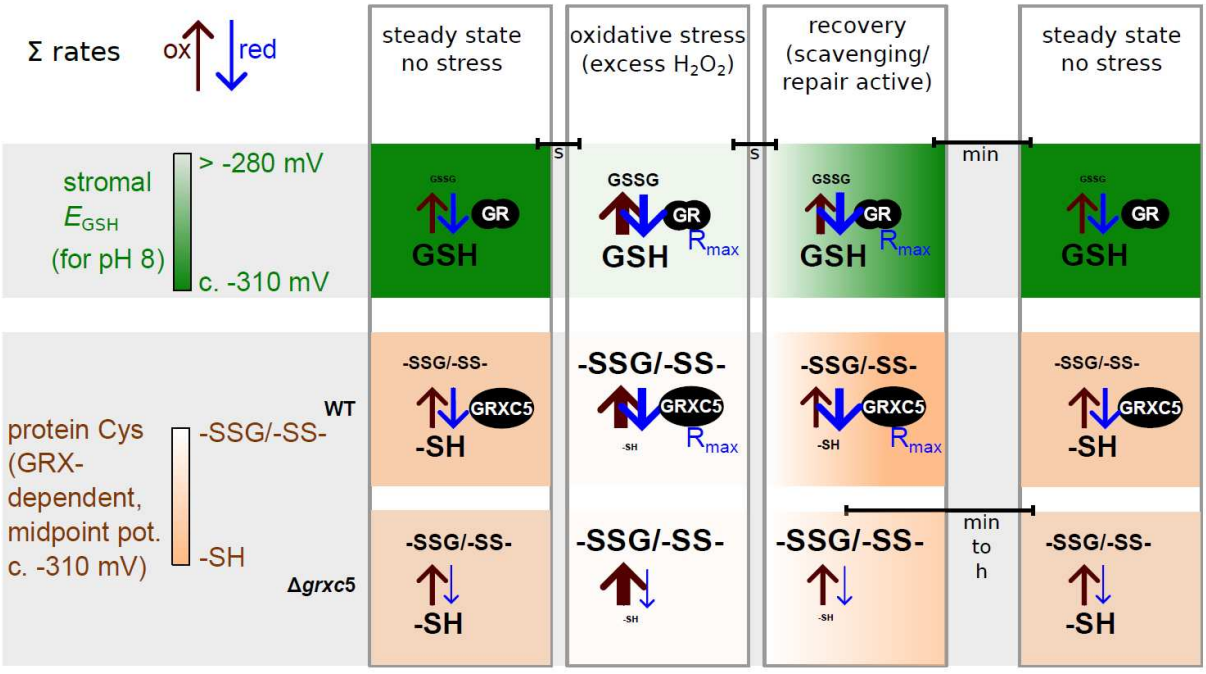

Fig. 8: Schematic overview: Model of observed dynamic redox states as a consequence of changing oxidation and reduction rates

Simplified scheme of steady states of the GSH/GSSG redox couple and resulting E_{GSH}, as well as the protein thiol/disulfide and thiol/glutathionylated redox couples before, during and after an oxidative challenge, as investigated in this work using roGFP2. Redox potentials are given for pH 8 (midpoint potential of roGFP2 at pH 8 is -310 mV). Colour scales exemplify relative changes between reduced and oxidised forms. Bars indicate approximate durations of transitions. Arrow thickness indicates sum of oxidation rates (i.e. all direct oxidation (slow) and enzymatically catalysed oxidation (fast)) and sum of reduction rates that would result in the observed profile of redox dynamics. Lack of GRXC5 leads to more oxidised steady state for target cysteines, as well as slow recovery rates. Enzymes are depicted as black ovals. R_{max} = maximal reachable reduction rate with current enzyme copy number.

Moreover, by generating Δ*grxc5*/Δ*gr1* double mutant lines, we found that GRXC5 function is not a main cause for the stress-sensitive and dwarfed Δ*gr1* phenotype. This excludes GRXC5 as main GSSG-producing enzyme in the stroma, as well as putatively toxic GRX-dependent *S*-glutathionylations occurring in response to an oxidatively shifted E_{GSH}. Glutathione can serve as electron donor for additional stromal enzymes involved in ROS-induced damage repair, signalling or ROS scavenging, such as plastidial MSRB1 (1 Cys methionine sulfoxide reductase B1) (Laugier et al., 2009), PRXIIE (Gama et al., 2008), GST iota/lambda (GSH *S*-transferase) and DHAR (dehydroascorbate reductase) (reviewed in (Müller-Schüssele et al., 2021a). These processes represent additional candidates for stroma-localised GSSG generation (see GSH oxidation rates in **Fig. 8**), and merit further investigation identifying their specific contributions to stress tolerance.

Is class I GRX function relevant in the chloroplast stroma?

TRX and GRX functions are partially redundant in *E. coli*, mostly related to their function as alternative electron donors to ribonucleotide reductase, powering cell growth (Fernandes and Holmgren, 2004). In the cytosol of *S. cerevisiae*, Δ*grx1*/Δ*grx2* null mutants grow normally but show increased sensitivity to oxidative challenge (Luikenhuis et al., 1998; Eckers et al., 2009). Lethality only occurred when concomitantly knocking-out all cytosolic TRX isoforms (Draculic et al., 2000). GRXs can operate through a monothiol mechanism or a dithiol mechanism in which only the N-terminal active site cysteine or both active site cysteines participate in the redox process, respectively (Lillig and Berndt, 2013). One cytosolic monothiol GRX was able and sufficient to compensate for loss of all TRX and GRX (Zimmermann et al., 2020). Partial redundancy between the GSH/GRX and TRX redox systems was also demonstrated in plants, regarding the cytosol and mitochondrial matrix (Marty et al., 2009), but not for the plastid stroma (Marty et al., 2019). Regarding mutants lacking all class I GRX of one compartment, double null mutants of *A. thaliana* lacking cytosolic GRXC1 and GRXC2 were originally described to be lethal (Riondet et al., 2012) but have recently been reported to be viable and with a WT-like phenotype (Schlößer et al., 2023). In the secretory pathway, which lacks a GR and thus possesses a less reducing E_{GSH}, double mutants of GRXC3/GRXC4 grow normally (Schlößer et al., 2023) but showed decreased hypocotyl length compared to WT when grown in elevated temperature (Dard et al., 2022). Regarding plastid-targeted class I GRX, no null

673 mutants were described yet. PpGRXC5 has a CPYC active site and could operate via the
674 monothiol or the dithiol mechanism (Deponte, 2017; Zimmermann et al., 2020). During land
675 plant evolution, a second isoform of plastid-targeted class I GRX lacking the second active site
676 Cys, GRXS12, evolved within the same clade (Müller-Schüssele et al., 2021a). Poplar
677 GRXS12 was characterized as functional monothiol class I GRX (Couturier et al., 2009;
678 Zaffagnini et al., 2012a), but the biological relevance of either class I GRX plastid isoform
679 remains so far unclear.
680 While E_{GSH} is usually robust, except under extreme abiotic stress conditions challenging GR
681 capacity (Wagner et al., 2019; Ugalde et al., 2021; Bohle et al., 2022) (**Fig. 8**), recent results
682 have shown that stromal E_{GSH} is dynamic in response to physiological light/dark transitions
683 (Müller-Schüssele et al., 2020; Haber et al., 2021). We found that in Δ*grxc5* stroma, these light-
684 dependent E_{GSH} dynamics are not transferred anymore to glutathione-dependent disulfides,
685 such as in roGFP2 (**Fig. 7A**), raising the question which endogenous target disulfides may
686 respond differently (**Fig. 8**). As an obvious target for interference between the TRX and
687 GSH/GRX system in the stroma, we tested CO_2 release and uptake in WT compared to Δ*grxc5*
688 lines and found no significant differences under the tested conditions (**Fig. 7B**). In accordance
689 with the normal plant growth observed in Δ*grxc5* lines, this result indicates that TRX-dependent
690 redox regulation of the CBB cycle (TRX-*m* and TRX-*f* isoforms) is not affected. This confirms
691 limited cross-talk between the TRX and class I GRX in the plastid stroma.
692 The remaining question is why GSH/GRX and TRX-dependent redox cascades can remain
693 largely separated in the same subcellular compartment. One possible explanation is substrate
694 specificity, e.g. mediated by electrostatic complementarity between redoxins and their target
695 proteins (Bodnar et al., 2023). As at least one stromal class I GRX isoform (GRXC5 or
696 GRXS12) is evolutionarily strictly conserved, an important function is likely, but may not consist
697 in backing-up TRX-dependent redox cascades. In accordance, plastid-localised PRXIIE that is
698 efficiently reduced via class I GRX, does not function as TRX oxidase like other PRX (Telman
699 et al., 2020).

700 ***S*-glutathionylation: A needle in the haystack or important PTM?**
701 A remaining important question is for which plastid processes fast GRX-mediated reduction
702 kinetics of either protein *S*-glutathionylation or GSH-dependent protein disulfides would matter.
703 By exogenously challenging plants with H_2O_2, we found that kinetically fast roGFP2 reduction
704 was absent in the stroma. This leads to prolonged disulfide persistence in a time frame of at
705 least 30 min after such an oxidative challenge, as well as to an altered steady state OxD.
706 Thermodynamic equilibration of purified proteins with E_{GSH} can take hours (Meyer et al., 2007).
707 In contrast, stromal roGFP2 oxidation kinetics after addition of H_2O_2 were not slower **(Fig. 5B)**.
708 Disulfides can be directly induced by H_2O_2, with the rate constant being dependent on the pK_a
709 of the more reactive cysteine (Zaffagnini et al., 2019a). In this case, the thiolate anion reacts

with H_2O_2, forming a sulfenic acid (-SOH) and water. This sulfenic acid can react with a nearby thiol, forming a disulfide (and water). In the presence of GSH, this reaction sequence can lead to GRX-independent *S*-glutathionylation. Using an anti-GSH antibody on stressed and control samples of WT and Δ*grxc5* lines we found increased total *S*-glutathionylation after oxidative challenge. Lack of GRXC5 did not interfere with the level of glutathionylated proteins after oxidative stress treatment (**Fig. 6, Fig. S8**), indicating a minor contribution of GRXC5-mediated *S*-glutathionylation under the tested conditions. Our results support the hypothesis that the most likely scenario for protein *S*-glutathionylation (and *S*-glutathionylation-dependent disulfide formation) *in vivo* involves activated thiol derivatives such as sulfenic acids, most efficiently formed on cysteine residues that are in a deprotonated state (*i.e.*, thiolates) at physiological pH (Zaffagnini et al., 2012b).

Previous studies have revealed around 150 stromal proteins as potential *S*-glutathionylation targets, using different experimental approaches (reviewed in Zaffagnini et al. (2019a) and Müller-Schüssele et al. (2021a)). However, it is still unclear under which physiological conditions which fraction of principally susceptible cysteine residues really is *S*-glutathionylated *in vivo*, including consequences to activity, stability or localization of the affected protein molecules. If *S*-glutathionylation only occurs for a minor fraction of proteins or a minor fraction of protein molecules of one protein isoform, effects on metabolic fluxes would be unlikely, as there are still many non-glutathionylated protein molecules present in the entire population. However, protein cysteines with stable thiolate anions are interesting candidates to sense H_2O_2 or GSSG levels in signalling processes, with reduction rates mediated via class I GRX. In this regard, cytosolic GAPDH provides an interesting example. This enzyme contains a reactive cysteine which is essential for catalysis and is a major target of H_2O_2-dependent oxidation (Trost et al., 2017; Talwar et al., 2023). The subsequent reaction of GSH with the sulfenylated catalytic cysteine induces *S*-glutathionylation and protects the enzyme from irreversible oxidation. However, the persistence of the glutathionylated state, which causes an unavoidable loss of function, has a drastic and irreversible effect on structural stability inducing protein misfolding and aggregation (Zaffagnini et al., 2019b).

In order to understand the biological relevance of protein *S*-glutathionylation as PTM in the chloroplast stroma, identification of *in vivo* targets of GRXC5 (and/or GRXS12 in angiosperms) is necessary. This task will require fitting methodological tools for high-throughput protein redox state analysis in combination with suitable mutants and time frames. Life imaging with genetically encoded redox sensors can meet the challenge to follow oxidation and reduction rates *in vivo*, and to effectively dose stress treatments.

Based on our results, we conclude that stromal class I GRX are necessary to quickly release *S*-glutathionylation or disulfides formed via an *S*-glutathionylation intermediate. The question of why GRX-assisted glutathione-dependent catalysis evolved (Deponte, 2013; Deponte,

2022) is still open, especially regarding the plastid stroma. The main difference of mutants lacking class I GRX in comparison to mutants lacking GR may be that there is still sufficiently high GSH (and sufficiently low GSSG) for GSH-dependent (GRX-independent) reduction. In absence of class I GRX activity, reduction of disulfides still occurs, but at lower rates driven by thermodynamics (**Fig. 8**).

In conclusion, the most likely class I GRX functions remain thiol protection and enzyme regulation in response to oxidative challenge (Fernandes and Holmgren, 2004; Berndt et al., 2014). Potentially, fast kinetic equilibration with E_{GSH} is just relevant for enzymes with an *S*-glutathionylation intermediate on catalytic cysteines, as they would be temporarily "locked" in their disulfide or -SSG form in absence of a class I GRX. In the stroma, 1Cys MSRB1 and PRXIIE are interesting candidates. Alternatively, protein Cys with low pK_a could have evolved on proteins involved in (moonlighting) signalling functions in response to oxidative challenge, which still await identification as specific GRX interaction partners.

Competing Interest

The authors declare that they have no conflicts of interest.

Author Contributions

FB, MZ, PT, AJM and SJM-S designed the research. FB, JR, SST, HJ, FR, AB, SB, OT, MS, SK performed experiments and analysed data. SJM-S, MSchw., AJM, PJ, MD, EN, MZ, PT supervised the research and provided resources.

FB and SJMS wrote the manuscript with contributions from all authors. All authors approved the manuscript before submission.

Data Availability

All data needed to evaluate the conclusions in the paper are present in the paper and/or the Supporting Information.

Acknowledgements

We thank Andreas Werle-Rutter (Molecular Botany RPTU), Maria Homagk (Chemical Signalling, INRES, University of Bonn) and Bastian Welter (University of Cologne) for technical assistance, as well as Prof. Frank Hochholdinger for support. We thank Dr. Marlene Elsässer and Dr. Mareike Schallenberg-Rüdinger for generating a Gateway version of the *PTA2_Act5* expression vector.

This work was supported by the DFG-funded Research Training Group GRK2064: 'Water use efficiency and drought stress responses: From Arabidopsis to Barley' (AJM, MSchw., FB and

779 SJM-S) and via the Joint Mobility Program between the DAAD (PPP Italy 57397466) and the
780 MIUR (Prog. n. 34433) (AJM and PT). JR was supported by a PhD grant from the University
781 of Bologna (PhD programs in Cellular Molecular Biology). Research in SK´s laboratory if
782 funded by DFG under Germany's Excellence Strategy – EXC 2048/1 – project 390686111.
783 SJM-S and OT are grateful for funding obtained from BioComp 3.0 'Dynamic Membrane
784 Processes in Biological Systems'. HJ, ST and SJM-S are grateful for support by the DFG-
785 funded Research Training Group GRK2737 'STRESSistance'.

786 # Literature

787 Alboresi A, Storti M, Morosinotto T (2019) Balancing protection and efficiency in the regulation
788 of photosynthetic electron transport across plant evolution. New Phytol 221: 105–109

789 Aller I, Rouhier N, Meyer AJ (2013) Development of roGFP2-derived redox probes for
790 measurement of the glutathione redox potential in the cytosol of severely glutathione-
791 deficient *rml1* seedlings. Front Plant Sci 4: 506

792 Alvarez B, Salinas G (2022) Basic concepts of thiol chemistry and biology. Redox Chem. Biol.
793 Thiols. Elsevier, pp 1–18

794 Balsera M, Uberegui E, Schürmann P, Buchanan BB (2014) Evolutionary Development of
795 Redox Regulation in Chloroplasts. Antioxid Redox Signal 21: 1327–1355

796 Bangash SAK, Müller-Schüssele SJ, Solbach D, Jansen M, Fiorani F, Schwarzländer M,
797 Kopriva S, Meyer AJ (2019) Low-glutathione mutants are impaired in growth but do not
798 show an increased sensitivity to moderate water deficit. PloS One 14: e0220589

799 Bedhomme M, Zaffagnini M, Marchand CH, Gao X-H, Moslonka-Lefebvre M, Michelet L,
800 Decottignies P, Lemaire SD (2009) Regulation by Glutathionylation of Isocitrate Lyase
801 from *Chlamydomonas reinhardtii*. J Biol Chem 284: 36282–36291

802 Begas P, Liedgens L, Moseler A, Meyer AJ, Deponte M (2017) Glutaredoxin catalysis requires
803 two distinct glutathione interaction sites. Nat Commun 8: 14835

804 Begas P, Staudacher V, Deponte M (2015) Systematic re-evaluation of the bis(2-hydroxyethyl)
805 disulfide (HEDS) assay reveals an alternative mechanism and activity of glutaredoxins.
806 Chem Sci 6: 3788–3796

807 Berndt C, Lillig CH, Flohé L (2014) Redox regulation by glutathione needs enzymes. Front
808 Pharmacol. *5*, 168.

809 Bodnar Y, Gellert M, Hossain FM, Lillig CH (2023) Breakdown of *Arabidopsis thaliana*
810 thioredoxins and glutaredoxins based on electrostatic similarity–Leads to common and
811 unique interaction partners and functions. PLOS ONE 18: e0291272

812 Bohle F, Klaus A, Tegethof H, Schwarzländer M, Hochholdinger F, Meyer AJ, Acosta IF,
813 Müller-Schüssele SJ (2022) High robustness of cytosolic glutathione redox potential
814 under combined salt and osmotic stress in barley as revealed by the biosensor Grx1-
815 roGFP2. bioRxiv doi: 10.1101/2022.12.22.521445

816 Bohle F, Meyer AJ, Mueller-Schuessele SJ (2023) Quantification of Redox-Sensitive GFP
817 Cysteine Redox State via Gel-Based Read-Out. *In* M Sharma, ed, Fluoresc. Proteins.
818 Springer US, New York, NY, pp 259–268

819 Bradford MM (1976) A rapid and sensitive method for the quantitation of microgram quantities
820 of protein utilizing the principle of protein-dye binding. Anal Biochem 72: 248–254

821 Buchanan BB, Balmer Y (2005) REDOX REGULATION: A Broadening Horizon. Annu Rev
822 Plant Biol 56: 187–220

823 Buchanan BB, Holmgren A, Jacquot J-P, Scheibe R (2012) Fifty years in the thioredoxin field
824 and a bountiful harvest. Biochim Biophys Acta BBA - Gen Subj 1820: 1822–1829

825 Cassier-Chauvat C, Marceau F, Farci S, Ouchane S, Chauvat F (2023) The Glutathione
826 System: A Journey from Cyanobacteria to Higher Eukaryotes. Antioxid Basel Switz 12:
827 1199

828 Couturier J, Jacquot J-P, Rouhier N (2013) Toward a refined classification of class I dithiol
829 glutaredoxins from poplar: biochemical basis for the definition of two subclasses. Front
830 Plant Sci. 4, 518.

831 Couturier J, Koh CS, Zaffagnini M, Winger AM, Gualberto JM, Corbier C, Decottignies P,
832 Jacquot J-P, Lemaire SD, Didierjean C, et al (2009) Structure-Function Relationship of
833 the Chloroplastic Glutaredoxin S12 with an Atypical WCSYS Active Site. J Biol Chem
834 284: 9299–9310

835 Couturier J, Ströher E, Albetel A-N, Roret T, Muthuramalingam M, Tarrago L, Seidel T, Tsan
836 P, Jacquot J-P, Johnson MK, et al (2011) Arabidopsis chloroplastic glutaredoxin C5 as
837 a model to explore molecular determinants for iron-sulfur cluster binding into
838 glutaredoxins. J Biol Chem 286: 27515–27527

839 Dard A, Weiss A, Bariat L, Picault N, Pontvianne F, Riondet C, Reichheld J-P (2022)
840 Glutathione-mediated plant response to high-temperature. bioRxiv doi:
841 10.1101/2022.03.28.485658

842 Deponte M (2017) The incomplete glutathione puzzle: Just guessing at numbers and figures?
843 Antioxid Redox Signal 27: 1130–1161

844 Deponte M (2022) Glutathione and glutathione-dependent enzymes. Redox Chem. Biol.
845 Thiols. Elsevier, pp 241–275

846 Deponte M (2013) Glutathione catalysis and the reaction mechanisms of glutathione-
847 dependent enzymes. Biochim Biophys Acta BBA - Gen Subj 1830: 3217–3266

848 Dooley CT, Dore TM, Hanson GT, Jackson WC, Remington SJ, Tsien RY (2004) Imaging
849 dynamic redox changes in mammalian cells with green fluorescent protein indicators.
850 J Biol Chem 279: 22284–22293

851 Draculic T, Dawes IW, Grant CM (2000) A single glutaredoxin or thioredoxin gene is essential
852 for viability in the yeast *Saccharomyces cerevisiae*. Mol Microbiol 36: 1167–1174

853 Eckers E, Bien M, Stroobant V, Herrmann JM, Deponte M (2009) Biochemical Characterization
854 of Dithiol Glutaredoxin 8 from *Saccharomyces cerevisiae*: The Catalytic Redox
855 Mechanism Redux. Biochemistry 48: 1410–1423

856 Fernandes AP, Holmgren A (2004) Glutaredoxins: Glutathione-Dependent Redox Enzymes
857 with Functions Far Beyond a Simple Thioredoxin Backup System. Antioxid Redox
858 Signal 6: 63–74

859 Fricker MD (2016) Quantitative redox imaging software. Antioxid Redox Signal 24: 752–762

Gama F, Bréhélin C, Gelhaye E, Meyer Y, Jacquot J-P, Rey P, Rouhier N (2008) Functional analysis and expression characteristics of chloroplastic Prx IIE. Physiol Plant 133: 599–610

Geigenberger P, Thormählen I, Daloso DM, Fernie AR (2017) The Unprecedented Versatility of the Plant Thioredoxin System. Trends Plant Sci 22: 249–262

Gurrieri L, Sparla F, Zaffagnini M, Trost P (2023) Dark complexes of the Calvin-Benson cycle in a physiological perspective. Semin Cell Dev Biol S1084-9521(23)00049–6

Gütle DD, Roret T, Müller SJ, Couturier J, Lemaire SD, Hecker A, Dhalleine T, Buchanan BB, Reski R, Einsle O, et al (2016) Chloroplast FBPase and SBPase are thioredoxin-linked enzymes with similar architecture but different evolutionary histories. Proc Natl Acad Sci U S A 113: 6779–6784

Gutscher M, Pauleau A-L, Marty L, Brach T, Wabnitz GH, Samstag Y, Meyer AJ, Dick TP (2008) Real-time imaging of the intracellular glutathione redox potential. Nat Methods 5: 553–559

Haber Z, Lampl N, Meyer AJ, Zelinger E, Hipsch M, Rosenwasser S (2021) Resolving diurnal dynamics of the chloroplastic glutathione redox state in Arabidopsis reveals its photosynthetically derived oxidation. Plant Cell 33: 1828–1844

Hohe A, Egener T, Lucht JM, Holtorf H, Reinhard C, Schween G, Reski R (2004) An improved and highly standardised transformation procedure allows efficient production of single and multiple targeted gene-knockouts in a moss, *Physcomitrella patens*. Curr Genet 44: 339–347

Kubo M, Imai A, Nishiyama T, Ishikawa M, Sato Y, Kurata T, Hiwatashi Y, Reski R, Hasebe M (2013) System for Stable β-Estradiol-Inducible Gene Expression in the Moss *Physcomitrella patens*. PloS One 8: e77356

Laugier E, Tarrago L, Vieira Dos Santos C, Eymery F, Havaux M, Rey P (2009) *Arabidopsis thaliana* plastidial methionine sulfoxide reductases B, MSRBs, account for most leaf peptide MSR activity and are essential for growth under environmental constraints through a role in the preservation of photosystem antennae. Plant J 61: 271–282

Lillig CH, Berndt C (2013) Cellular functions of glutathione. Biochim Biophys Acta BBA - Gen Subj 1830: 3137–3138

Lillig CH, Berndt C, Holmgren A (2008) Glutaredoxin systems. Biochim Biophys Acta BBA - Gen Subj 1780: 1304–1317

Luikenhuis S, Perrone G, Dawes IW, Grant CM (1998) The Yeast *Saccharomyces cerevisiae* Contains Two Glutaredoxin Genes That Are Required for Protection against Reactive Oxygen Species. Mol Biol Cell 9: 1081–1091

Marri L, Thieulin-Pardo G, Lebrun R, Puppo R, Zaffagnini M, Trost P, Gontero B, Sparla F (2014) CP12-mediated protection of Calvin-Benson cycle enzymes from oxidative stress. Biochimie 97: 228–237

Marty L, Bausewein D, Müller C, Bangash SAK, Moseler A, Schwarzländer M, Müller-Schüssele SJ, Zechmann B, Riondet C, Balk J, et al (2019) Arabidopsis glutathione reductase 2 is indispensable in plastids, while mitochondrial glutathione is safeguarded by additional reduction and transport systems. New Phytol 224: 1569–1584

902 Marty L, Siala W, Schwarzlander M, Fricker MD, Wirtz M, Sweetlove LJ, Meyer Y, Meyer AJ,
903 Reichheld J-P, Hell R (2009) The NADPH-dependent thioredoxin system constitutes a
904 functional backup for cytosolic glutathione reductase in Arabidopsis. Proc Natl Acad
905 Sci 106: 9109–9114

906 Meyer AJ, Brach T, Marty L, Kreye S, Rouhier N, Jacquot J-P, Hell R (2007) Redox-sensitive
907 GFP in *Arabidopsis thaliana* is a quantitative biosensor for the redox potential of the
908 cellular glutathione redox buffer. Plant J 52: 973–986

909 Meyer AJ, Dick TP (2010) Fluorescent protein-based redox probes. Antioxid Redox Signal 13:
910 621–650

911 Meyer AJ, Dreyer A, Ugalde JM, Feitosa-Araujo E, Dietz K-J, Schwarzländer M (2021) Shifting
912 paradigms and novel players in Cys-based redox regulation and ROS signaling in
913 plants - and where to go next. Biol Chem 402: 399–423

914 Michelet L, Zaffagnini M, Marchand C, Collin V, Decottignies P, Tsan P, Lancelin J-M, Trost P,
915 Miginiac-Maslow M, Noctor G, et al (2005) Glutathionylation of chloroplast thioredoxin
916 f is a redox signaling mechanism in plants. Proc Natl Acad Sci 102: 16478–16483

917 Michelet L, Zaffagnini M, Morisse S, Sparla F, Pérez-Pérez ME, Francia F, Danon A, Marchand
918 CH, Fermani S, Trost P, et al (2013) Redox regulation of the Calvin-Benson cycle:
919 something old, something new. Front Plant Sci 4: 470

920 Morales A, Kaiser E (2020) Photosynthetic Acclimation to Fluctuating Irradiance in Plants.
921 Front Plant Sci 11: 268

922 Mueller SJ, Lang D, Hoernstein SNW, Lang EGE, Schuessele C, Schmidt A, Fluck M,
923 Leisibach D, Niegl C, Zimmer AD, et al (2014) Quantitative analysis of the mitochondrial
924 and plastid proteomes of the moss *Physcomitrella patens* reveals protein
925 macrocompartmentation and microcompartmentation. Plant Physiol 164: 2081–2095

926 Mueller SJ, Reski R (2015) Mitochondrial Dynamics and the ER: The Plant Perspective. Front
927 Cell Dev Biol 3: 78

928 Müller-Schüssele SJ, Bohle F, Rossi J, Trost P, Meyer AJ, Zaffagnini M (2021a) Plasticity in
929 plastid redox networks: evolution of glutathione-dependent redox cascades and
930 glutathionylation sites. BMC Plant Biol 21: 322

931 Müller-Schüssele SJ, Schwarzländer M, Meyer AJ (2021b) Live monitoring of plant redox and
932 energy physiology with genetically encoded biosensors. Plant Physiol 186: 93–109

933 Müller-Schüssele SJ, Wang R, Gütle DD, Romer J, Rodriguez-Franco M, Scholz M, Buchert
934 F, Lüth VM, Kopriva S, Dörmann P, et al (2020) Chloroplasts require glutathione
935 reductase to balance reactive oxygen species and maintain efficient photosynthesis.
936 Plant J 103: 1140–1154

937 Noctor G, Mhamdi, A, Chaouch S, Han Y, Neukermans J, Marquez-Garcia B, Queval G, Foyer
938 CH (2012) Glutathione in plants: an integrated overview: glutathione status and functions.
939 *Plant, Cell & Environment* 35: 454–484.

940 Ojeda V, Pérez-Ruiz JM, Cejudo FJ (2018) 2-Cys Peroxiredoxins Participate in the Oxidation
941 of Chloroplast Enzymes in the Dark. Mol Plant 11: 1377–1388

Pérez-Ruiz JM, Naranjo B, Ojeda V, Guinea M, Cejudo FJ (2017) NTRC-dependent redox balance of 2-Cys peroxiredoxins is needed for optimal function of the photosynthetic apparatus. Proc Natl Acad Sci U S A 114: 12069–12074

Reski R, Abel WO (1985) Induction of budding on chloronemata and caulonemata of the moss, *Physcomitrella patens*, using isopentenyladenine. Planta 165: 354–358

Riondet C, Desouris JP, Montoya JG, Chartier Y, Meyer Y, Reichheld J-P (2012) A dicotyledon-specific glutaredoxin GRXC1 family with dimer-dependent redox regulation is functionally redundant with GRXC2. Plant Cell Environ 35: 360–373

Roach T, Krieger-Liszkay A (2014) Regulation of photosynthetic electron transport and photoinhibition. Curr Protein Pept Sci 15: 351–362

Rouhier N, Unno H, Bandyopadhyay S, Masip L, Kim S-K, Hirasawa M, Gualberto JM, Lattard V, Kusunoki M, Knaff DB, et al (2007) Functional, structural, and spectroscopic characterization of a glutathione-ligated [2Fe–2S] cluster in poplar glutaredoxin C1. Proc Natl Acad Sci 104: 7379–7384

Schlößer M, Moseler A, Bodnar Y, Homagk M, Wagner S, Pedroletti L, Gellert M, Ugalde JM, Lillig CH, Meyer AJ (2023) Localization of four class I glutaredoxins in the cytosol and the secretory pathway and characterization of their biochemical diversification. bioRxiv doi: 10.1101/2023.09.01.555924

Schöttler MA, Toth SZ (2014) Photosynthetic complex stoichiometry dynamics in higher plants: environmental acclimation and photosynthetic flux control. Front Plant Sci 5: 188

Schreiber M, Rensing SA, Gould SB (2022) The greening ashore. Trends Plant Sci 27: 847–857

Schwarzländer M, Dick TP, Meyer AJ, Morgan B (2016) Dissecting redox biology using fluorescent protein sensors. Antioxid Redox Signal 24: 680–712

Schwarzländer M, Fricker MD, MüLler C, Marty L, Brach T, Novak J, Sweetlove LJ, Hell R, Meyer AJ (2008) Confocal imaging of glutathione redox potential in living plant cells. J Microsc 231: 299–316

Speiser A, Silbermann M, Dong Y, Haberland S, Uslu VV, Wang S, Bangash SAK, Reichelt M, Meyer AJ, Wirtz M, et al (2018) Sulfur Partitioning between Glutathione and Protein Synthesis Determines Plant Growth. Plant Physiol 177: 927–937

Talwar D, Miller CG, Grossmann J, Szyrwiel L, Schwecke T, Demichev V, Mikecin Drazic A-M, Mayakonda A, Lutsik P, Veith C, et al (2023) The GAPDH redox switch safeguards reductive capacity and enables survival of stressed tumor cells. Nat Metab 5: 660–676

Teh JT, Leitz V, Holzer VJC, Neusius D, Marino G, Meitzel T, García-Cerdán JG, Dent RM, Niyogi KK, Geigenberger P, et al (2023) NTRC regulates CP12 to activate Calvin-Benson cycle during cold acclimation. Proc Natl Acad Sci U S A 120: e2306338120

Telman W, Liebthal M, Dietz K-J (2020) Redox regulation by peroxiredoxins is linked to their thioredoxin-dependent oxidase function. Photosynth Res 145: 31–41

Tian G-W, Mohanty A, Chary SN, Li S, Paap B, Drakakaki G, Kopec CD, Li J, Ehrhardt D, Jackson D, et al (2004) High-throughput fluorescent tagging of full-length Arabidopsis gene products in planta. Plant Physiol 135: 25–38

983 Trnka D, Engelke AD, Gellert M, Moseler A, Hossain MF, Lindenberg TT, Pedroletti L,
984 Odermatt B, de Souza JV, Bronowska AK, et al (2020) Molecular basis for the distinct
985 functions of redox-active and FeS-transfering glutaredoxins. Nat Commun 11: 3445

986 Trost P, Fermani S, Calvaresi M, Zaffagnini M (2017) Biochemical basis of sulphenomics: how
987 protein sulphenic acids may be stabilized by the protein microenvironment. Plant Cell
988 Environ 40: 483–490

989 Ugalde JM, Fuchs P, Nietzel T, Cutolo EA, Homagk M, Vothknecht UC, Holuigue L,
990 Schwarzländer M, Müller-Schüssele SJ, Meyer AJ (2021) Chloroplast-derived photo-
991 oxidative stress causes changes in H_2O_2 and E_{GSH} in other subcellular compartments.
992 Plant Physiol 186: 125–141

993 Vaseghi M-J, Chibani K, Telman W, Liebthal MF, Gerken M, Schnitzer H, Mueller SM, Dietz
994 K-J (2018) The chloroplast 2-cysteine peroxiredoxin functions as thioredoxin oxidase
995 in redox regulation of chloroplast metabolism. eLife 7: 38194

996 Wagner S, Steinbeck J, Fuchs P, Lichtenauer S, Elsässer M, Schippers JHM, Nietzel T,
997 Ruberti C, Van Aken O, Meyer AJ, et al (2019) Multiparametric real-time sensing of
998 cytosolic physiology links hypoxia responses to mitochondrial electron transport. New
999 Phytol 224: 1668–1684

1000 Wessel D, Flügge UI (1984) A method for the quantitative recovery of protein in dilute solution
1001 in the presence of detergents and lipids. Anal Biochem 138: 141–143

1002 Yoshida K, Yokochi Y, Hisabori T (2019) New Light on Chloroplast Redox Regulation:
1003 Molecular Mechanism of Protein Thiol Oxidation. Front Plant Sci 10: 1534

1004 Yu X, Pasternak T, Eiblmeier M, Ditengou F, Kochersperger P, Sun J, Wang H, Rennenberg
1005 H, Teale W, Paponov I, et al (2013) Plastid-Localized Glutathione Reductase2-
1006 Regulated Glutathione Redox Status Is Essential for Arabidopsis Root Apical Meristem
1007 Maintenance. Plant Cell 25: 4451–4468

1008 Zaffagnini M, Bedhomme M, Marchand CH, Couturier JRM, Gao X-H, Rouhier N, Trost P,
1009 Lemaire SPD (2012a) Glutaredoxin S12: unique properties for redox signaling. Antioxid
1010 Redox Signal 16: 17–32

1011 Zaffagnini M, Bedhomme M, Marchand CH, Morisse S, Trost P, Lemaire SD (2012b) Redox
1012 regulation in photosynthetic organisms: Focus on glutathionylation. Antioxid Redox
1013 Signal 16: 567–586

1014 Zaffagnini M, Fermani S, Costa A, Lemaire SD, Trost P (2013) Plant cytoplasmic GAPDH:
1015 Redox post-translational modifications and moonlighting properties. Front Plant Sci.
1016 doi: 10.3389/fpls.2013.00450

1017 Zaffagnini M, Fermani S, Marchand CH, Costa A, Sparla F, Rouhier N, Geigenberger P,
1018 Lemaire SD, Trost P (2019a) Redox Homeostasis in Photosynthetic Organisms: Novel
1019 and Established Thiol-Based Molecular Mechanisms. Antioxid Redox Signal 31: 155–
1020 210

1021 Zaffagnini M, Marchand CH, Malferrari M, Murail S, Bonacchi S, Genovese D, Montalti M,
1022 Venturoli G, Falini G, Baaden M, et al (2019b) Glutathionylation primes soluble
1023 glyceraldehyde-3-phosphate dehydrogenase for late collapse into insoluble
1024 aggregates. Proc Natl Acad Sci 116: 26057–26065

Zaffagnini M, Michelet L, Marchand C, Sparla F, Decottignies P, Le Maréchal P, Miginiac-Maslow M, Noctor G, Trost P, Lemaire SD (2007) The thioredoxin-independent isoform of chloroplastic glyceraldehyde-3-phosphate dehydrogenase is selectively regulated by glutathionylation. FEBS J 274: 212–226

Zaffagnini M, Michelet L, Massot V, Trost P, Lemaire SD (2008) Biochemical Characterization of Glutaredoxins from *Chlamydomonas reinhardtii* Reveals the Unique Properties of a Chloroplastic CGFS-type Glutaredoxin. J Biol Chem 283: 8868–8876

Zimmer D, Swart C, Graf A, Arrivault S, Tillich M, Proost S, Nikoloski Z, Stitt M, Bock R, Mühlhaus T, et al (2021) Topology of the redox network during induction of photosynthesis as revealed by time-resolved proteomics in tobacco. Sci Adv 7: eabi8307

Zimmermann J, Oestreicher J, Hess S, Herrmann JM, Deponte M, Morgan B (2020) One cysteine is enough: A monothiol Grx can functionally replace all cytosolic Trx and dithiol Grx. Redox Biol 36: 101598

Supporting Information

Fig. S1: Construct design and knock-out validation

Fig. S2: Fresh weight analysis for Δ*grxc5*, Δ*gr1* and Δ*grxc5*/Δ*gr1*

Fig. S3: Stress phenotyping of P.patens protonema culture under fluctuating light and heat stress

Fig. S4: Non-photochemical quenching (NPQ) measurements of 4-week-old gametophores under low and high light regimes

Fig. S5: Targeting of roGFP2 to plastids

Fig. S6: Quantification of total GSH in GRXC5 mutant lines by HPLC

Fig. S7: roGFP2 oxidation state and recovery in response to externally added H_2O_2

Fig. S8: Increase of protein-bound glutathione after H_2O_2 treatment

Table S1: Primer sequences

Supplementary Material and Methods:

Measurement of photosynthetic parameters (light induction and relaxation curves)

Glutathione measurement by HPLC